J|A|C|S
ARTICLES
Published on Web 11/02/2005

Imido Transfer from Bis(imido)ruthenium(VI) Porphyrins to Hydrocarbons: Effect of Imido Substituents, C−H Bond Dissociation Energies, and $Ru^{VI/V}$ Reduction Potentials

Sarana Ka-Yan Leung, Wai-Man Tsui, Jie-Sheng Huang,* Chi-Ming Che,* Jiang-Lin Liang, and Nianyong Zhu

Contribution from the Department of Chemistry and Open Laboratory of Chemical Biology of the Institute of Molecular Technology for Drug Discovery and Synthesis, The University of Hong Kong, Pokfulam Road, Hong Kong

Received June 29, 2005; E-mail: cmche@hku.hk; jshuang@hku.hk

Abstract: $[Ru^{VI}(TMP)(NSO_2R)_2]$ (SO_2R = Ms, Ts, Bs, Cs, Ns; R = *p*-C_6H_4OMe, *p*-C_6H_4Me, C_6H_5, *p*-C_6H_4Cl, *p*-$C_6H_4NO_2$, respectively) and $[Ru^{VI}(Por)(NTs)_2]$ (Por = 2,6-Cl_2TPP, F_{20}-TPP) were prepared by the reactions of $[Ru^{II}(Por)(CO)]$ with $PhI{=}NSO_2R$ in CH_2Cl_2. These complexes exhibit reversible $Ru^{VI/V}$ couple with $E_{1/2} = -0.41$ to -0.12 V vs $Cp_2Fe^{+/0}$ and undergo imido transfer reactions with styrenes, norbornene, *cis*-cyclooctene, indene, ethylbenzenes, cumene, 9,10-dihydroanthracene, xanthene, cyclohexene, toluene, and tetrahydrofuran to afford aziridines or amides in up to 85% yields. The second-order rate constants (k_2) of the aziridination/amidation reactions at 298 K were determined to be $(2.6 \pm 0.1) \times 10^{-5}$ to 14.4 ± 0.6 $dm^3\ mol^{-1}\ s^{-1}$, which generally increase with increasing $Ru^{VI/V}$ reduction potential of the imido complexes and decreasing C−H bond dissociation energy (BDE) of the hydrocarbons. A linear correlation was observed between log k' (k' is the k_2 value divided by the number of reactive hydrogens) and BDE and between log k_2 and $E_{1/2}(Ru^{VI/V})$; the linearity in the former case supports a H-atom abstraction mechanism. The amidation by $[Ru^{VI}(TMP)(NNs)_2]$ reverses the thermodynamic reactivity order cumene > ethylbenzene/toluene, with $k'(3°\ C{-}H)/k'(2°\ C{-}H) = 0.2$ and $k'(3°\ C{-}H)/k'(1°\ C{-}H) = 0.8$.

Introduction

The chemistry of metal-catalyzed aziridination of alkenes and amidation of C−H bonds using iminoiodane ($PhI{=}NSO_2R$), "$PhI(OAc)_2 + NH_2SO_2R$", or "$PhIO + NH_2SO_2R$" as nitrogen source, as depicted in reactions 1 and 2 (Figure 1), has expanded dramatically in the past decade.[1−26] Such catalytic processes are increasingly attractive as a synthetic route to aziridines or amides. The widely believed involvement of reactive metal imido (or nitrene) intermediates ($M{=}NSO_2R$ species) in reactions 1 and 2 places great importance on the investigation of their chemistry, particularly with regard to imido transfer

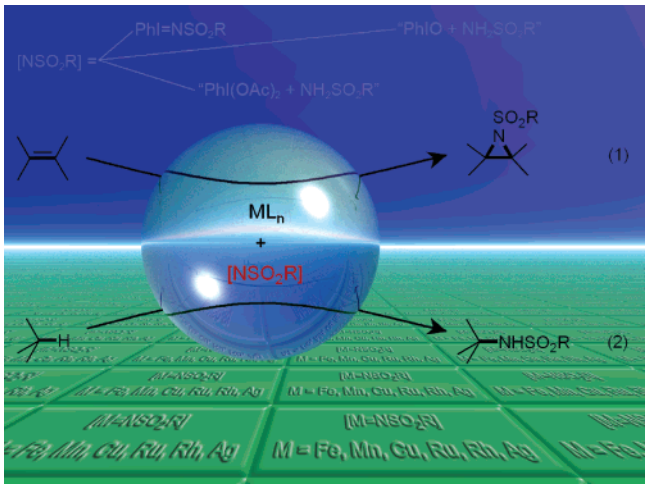

Figure 1. Metal-catalyzed aziridination of alkenes and amidation of C−H bonds using iminoiodane ($PhI{=}NSO_2R$), "$PhI(OAc)_2 + NH_2SO_2R$", or "$PhIO + NH_2SO_2R$" as nitrogen source. These processes are proposed to involve $M{=}NSO_2R$ intermediates.

(1) (a) Breslow, R.; Gellman, S. H. *J. Chem. Soc., Chem. Commun.* **1982**, 1400. (b) Breslow, R.; Gellman, S. H. *J. Am. Chem. Soc.* **1983**, *105*, 6728. (c) Yang, J.; Weinberg, R.; Breslow, R. *Chem. Commun.* **2000**, 531.
(2) (a) Mansuy, D.; Mahy, J.-P.; Dureault, A.; Bedi, G.; Battioni, P. *J. Chem. Soc., Chem. Commun.* **1984**, 1161. (b) Mahy, J.-P.; Bedi, G.; Battioni, P.; Mansuy, D. *J. Chem. Soc., Perkin Trans. 2* **1988**, 1517. (c) Mahy, J. P.; Bedi, G.; Battioni, P.; Mansuy, D. *Tetrahedron Lett.* **1988**, *29*, 1927. (d) Mahy, J. P.; Bedi, G.; Battioni, P.; Mansuy, D. *New J. Chem.* **1989**, *13*, 651.
(3) (a) Evans, D. A.; Faul, M. M.; Bilodeau, M. T. *J. Org. Chem.* **1991**, *56*, 6744. (b) Evans, D. A.; Faul, M. M.; Bilodeau, M. T.; Anderson, B. A.; Barnes, D. M. *J. Am. Chem. Soc.* **1993**, *115*, 5328. (c) Evans, D. A.; Faul, M. M.; Bilodeau, M. T. *J. Am. Chem. Soc.* **1994**, *116*, 2742.
(4) Li, Z.; Quan, R. W.; Jacobsen, E. N. *J. Am. Chem. Soc.* **1995**, *117*, 5889.
(5) (a) Müller, P.; Baud, C.; Jacquier, Y.; Moran, M.; Nägeli, I. *J. Phys. Org. Chem.* **1996**, *9*, 341. (b) Müller, P.; Baud, C.; Jacquier, Y. *Tetrahedron* **1996**, *52*, 1543. (c) Nägeli, I.; Baud, C.; Bernardinelli, G.; Jacquier, Y.; Moran, M.; Müller, P. *Helv. Chim. Acta* **1997**, *80*, 1087. (d) Müller, P.; Baud, C.; Nägeli, I. *J. Phys. Org. Chem.* **1998**, *11*, 597. (e) Müller, P.; Baud, C.; Jacquier, Y. *Can. J. Chem.* **1998**, *76*, 738. (f) Müller, P.; Fruit, C. *Chem. Rev.* **2003**, *103*, 2905. (g) Fruit, C.; Müller, P. *Tetrahedron: Asymmetry* **2004**, *15*, 1019. (h) Fruit, C.; Müller, P. *Helv. Chim. Acta* **2004**, *87*, 1607.
(6) (a) Nishikori, H.; Katsuki, T. *Tetrahedron Lett.* **1996**, *37*, 9245. (b) Kohmura, Y.; Katsuki, T. *Tetrahedron* Lett. **2001**, *42*, 3339.
(7) Harm, A. M.; Knight, J. G.; Stemp, G. *Tetrahedron Lett.* **1996**, *37*, 6189.
(8) (a) Södergren, M. J.; Alonso, D. A.; Andersson, P. G. *Tetrahedron: Asymmetry* **1997**, *8*, 3563. (b) Södergren, M. J.; Alonso, D. A.; Bedekar, A. V.; Andersson, P. G. *Tetrahedron Lett.* **1997**, *38*, 6897. (c) Bertilsson, S. K.; Tedenborg, L.; Alonso, D. A.; Andersson, P. G. *Organometallics* **1999**, *18*, 1281. (d) Brandt, P.; Södergren, M. J.; Andersson, P. G.; Norrby, P.-O. *J. Am. Chem. Soc.* **2000**, *122*, 8013.

reactions with alkenes and imido insertion into C−H bonds, which could provide valuable insight into the mechanism of metal-catalyzed aziridination/amidation reactions.

While a variety of iron,[1,2,12,22] manganese,[1,2,6,12] copper,[3,4,7−9,11,13−17,20,23−26] ruthenium,[10a−g,j,k] dirhodium,[5,10h,i,18,19] and silver[21] complexes have been demonstrated to be efficient catalysts for reactions 1 and/or 2, isolation or spectroscopic identification of putative M=NSO$_2$R species remains a serious challenge. In fact, well characterized M=NSO$_2$R complexes are sparse, including [Mo^{VI}O$_n$(NTs)$_{2-n}$(Et$_2$dtc)$_2$] (n = 0, 1),[27,28a,b] [Tp′(CO)$_2$W(NTs)][I$_3$],[28c,29] [Ru^{VI}(Por)(NTs)$_2$],[10f,30] and [Os^{VI}(Por)(NTs)$_2$],[31] of which only [Ru^{VI}(Por)(NTs)$_2$] can undergo alkene aziridination and C−H bond amidation.[10f,30]

Imido transfer reactions with alkenes have also been known for a few other types of metal imido complexes, including [Os^{VIII}O$_{4-n}$(NBu^t)$_n$] (n = 1−3)[32] and [Os^{VIII}O$_3$(NR)][32c] for oxyamination or diamination of alkenes, [Mn^{V}(TMP)(NCOCF$_3$)(OOCCF$_3$)] for aziridination of cyclooctene,[28d,33] and [(dtbpe)Ni=N(2,6-Pr$^i_2$C$_6$H$_3$)] for aziridination of ethylene.[28e,34]

Direct mechanistic studies on alkene aziridination and C−H bond amidation reactions of reactive metal imido complexes are rare. In a previous work,[30b] the reactions of [Ru^{VI}(TPP)(NTs)$_2$] [28f] with styrenes, norbornene, cyclohexene, cyclooctene, ethylbenzenes, and cumene were examined through kinetic studies. The observed effect of 1e oxidation potential of alkenes and the effect of para-substituents of styrenes or ethylbenzenes on rate constants, along with kinetic isotope effect, support rate-limiting formation of carboradical intermediates in the imido transfer reactions.[30b]

To gain further insight into the mechanism of alkene aziridination and C−H bond amidation, it would be of interest to examine the effect of reduction potentials of metal imido complexes and C−H bond dissociation energies (BDEs) of hydrocarbons on the reaction rate constants. *Such driving force dependence of rate constants, to our knowledge, has not hitherto been reported in metal imido chemistry, nor have electrochemical studies on reactive M=NSO$_2$R complexes been reported in the literature.* In metal oxo chemistry, Bruice,[35a] Che,[35b] and co-workers examined the effect of reduction potentials of metal oxo complexes on the rate constants of alkene epoxidation reactions; *Mayer and co-worker demonstrated the importance of BDE to the reaction rate constants of C−H bond oxidations.*[36] In view of the analogy between oxo and imido groups, an important issue to be addressed is whether the results obtained for metal oxo complexes can be extended to metal imido complexes.

On the other hand, imido groups have tunable steric hindrance and can be much bulkier than oxo groups, rendering C−H bond amidation by metal imido complexes to encounter larger steric hindrance than C−H bond oxidation by metal oxo complexes. Consequently, by replacing an oxo group with an imido group, it may be possible to reverse the thermodynamic reactivity order 3° > 2° > 1° C−H bonds without the need of altering the steric hindrance of auxiliary ligands. This unique approach to reversal of the relative reactivity of 3° versus 2° versus 1° C−H bonds has rarely been investigated.[30b]

(9) (a) Díaz-Requejo, M. M.; Pérez, P. J.; Brookhart, M.; Templeton, J. L. *Organometallics* **1997**, *16*, 4399. (b) Díaz-Requejo, M. M.; Belderraín, T. R.; Nicasio, M. C.; Trofimenko, S.; Pérez, P. J. *J. Am. Chem. Soc.* **2003**, *125*, 12078. (c) Mairena, M. A.; Díaz-Requejo, M. M.; Belderraín, T. R.; Nicasio, M. C.; Trofimenko, S.; Pérez, P. J. *Organometallics* **2004**, *23*, 253.

(10) (a) Lai, T.-S.; Kwong, H.-L.; Che, C.-M.; Peng, S.-M. *Chem. Commun.* **1997**, 2373. (b) Au, S.-M.; Zhang, S.-B.; Fung, W.-H.; Yu, W.-Y.; Che, C.-M.; Cheung, K.-K. *Chem. Commun.* **1998**, 2677. (c) Zhou, X.-G.; Yu, X.-Q.; Huang, J.-S.; Che, C.-M. *Chem. Commun*. **1999**, 2377. (d) Yu, X.-Q.; Huang, J.-S.; Zhou, X.-G.; Che, C.-M. *Org. Lett.* **2000**, *2*, 2233. (e) Au, S.-M.; Huang, J.-S.; Che, C.-M.; Yu, W.-Y. *J. Org. Chem.* **2000**, *65*, 7858. (f) Liang, J.-L.; Huang, J.-S.; Yu, X.-Q.; Zhu, N.; Che, C.-M. *Chem.—Eur. J.* **2002**, *8*, 1563. (g) Liang, J.-L.; Yuan, S.-X.; Huang, J.-S.; Yu, W.-Y.; Che, C.-M. *Angew. Chem., Int. Ed.* **2002**, *41*, 3465. (h) Liang, J.-L.; Yuan, S.-X.; Chan, P. W. H.; Che, C.-M. *Org. Lett.* **2002**, *4*, 4507. (i) Liang, J.-L.; Yuan, S.-X.; Chan, P. W. H.; Che, C.-M. *Tetrahedron Lett.* **2003**, *44*, 5917. (j) Liang, J.-L.; Yuan, S.-X.; Huang, J.-S.; Che, C.-M. *J. Org. Chem.* **2004**, *69*, 3610. (k) He, L.; Chan, P. W. H.; Tsui, W.-M.; Yu, W.-Y.; Che, C.-M. *Org. Lett.* **2004**, *6*, 2405.

(11) (a) Dauban, P.; Dodd, R. H. *Tetrahedron Lett.* **1998**, *39*, 5739. (b) Dauban, P.; Dodd, R. H. *J. Org. Chem.* **1999**, *64*, 5304. (c) Dauban, P.; Dodd, R. H. *Org. Lett*. **2000**, *2*, 2327. (d) Dauban, P.; Sanière, L.; Tarrade, A.; Dodd, R. H. *J. Am. Chem. Soc.* **2001**, *123*, 7707. (e) Duran, F.; Leman, L.; Ghini, A.; Burton, G.; Dauban, P.; Dodd, R. H. *Org. Lett*. **2002**, *4*, 2481. (f) Dauban, P.; Dodd, R. H. *Synlett* **2003**, 1571. (g) Sanière, L.; Leman, L.; Bourguignon, J.-J.; Dauban, P.; Dodd, R. H. *Tetrahedron* **2004**, *60*, 5889.

(12) Simonato, J.-P.; Pécaut, J.; Scheidt, W. R.; Marchon, J.-C. *Chem. Commun.* **1999**, 989.

(13) (a) Halfen, J. A.; Hallman, J. K.; Schultz, J. A.; Emerson, J. P. *Organometallics* **1999**, *18*, 5435. (b) Halfen, J. A.; Uhan, J. M.; Fox, D. C.; Mehn, M. P.; Que, L., Jr. *Inorg. Chem.* **2000**, *39*, 4913. (c) Halfen, J. A.; Fox, D. C.; Mehn, M. P.; Que, L., Jr. *Inorg. Chem.* **2001**, *40*, 5060.

(14) Adam, W.; Roschmann, K. J.; Saha-Möller, C. R. *Eur. J. Org. Chem.* **2000**, 557.

(15) Llewellyn, D. B.; Adamson, D.; Arndtsen, B. A. *Org. Lett.* **2000**, *2*, 4165.

(16) (a) Sanders, C. J.; Gillespie, K. M.; Bell, D.; Scott, P. *J. Am. Chem. Soc.* **2000**, *122*, 7132. (b) Gillespie, K. M.; Crust, E. J.; Deeth, R. J.; Scott, P. *Chem. Commun.* **2001**, 785. (c) Gillespie, K. M.; Sanders, C. J.; O'Shaughnessy, P.; Westmoreland, I.; Thickitt, C. P.; Scott, P. *J. Org. Chem.* **2002**, *67*, 3450.

(17) Taylor, S.; Gullick, J.; McMorn, P.; Bethell, D.; Page, P. C. B.; Hancock, F. E.; King, F.; Hutchings, G. J. *J. Chem. Soc., Perkin Trans. 2* **2001**, 1714.

(18) (a) Espino, C. G.; Wehn, P. M.; Chow, J.; Du Bois, J. *J. Am. Chem. Soc.* **2001**, *123*, 6935. (b) Guthikonda, K.; Du Bois, J. *J. Am. Chem. Soc.* **2002**, *124*, 13672. (c) Wehn, P. M.; Lee, J.; Du Bois, J. *Org. Lett.* **2003**, *5*, 4823. (d) Fiori, K. W.; Fleming, J. J.; Du Bois, J. *Angew. Chem., Int. Ed.* **2004**, *43*, 4349. (e) Espino, C. G.; Fiori, K. W.; Kim, M.; Du Bois, J. *J. Am. Chem. Soc.* **2004**, *126*, 15378.

(19) (a) Padwa, A.; Stengel, T. *Org. Lett.* **2002**, *4*, 2137. (b) Padwa, A.; Flick, A. C.; Leverett, C. A.; Stengel, T. *J. Org. Chem.* **2004**, *69*, 6377.

(20) Comba, P.; Merz, M.; Pritzkow, H. *Eur. J. Inorg. Chem.* **2003**, 1711.

(21) (a) Cui, Y.; He, C. *J. Am. Chem. Soc.* **2003**, *125*, 16202. (b) Cui, Y.; He, C. *Angew. Chem., Int. Ed.* **2004**, *43*, 4210.

(22) Avenier, F.; Latour, J.-M. *Chem. Commun.* **2004**, 1544.

(23) Xu, J.; Ma, L.; Jiao, P. *Chem. Commun.* **2004**, 1616.

(24) Leca, D.; Toussaint, A.; Mareau, C.; Fensterbank, L.; Lacôte, E.; Malacria, M. *Org. Lett.* **2004**, *6*, 3573.

(25) Han, H.; Bae, I.; Yoo, E. J.; Lee, J.; Do, Y.; Chang, S. *Org. Lett.* **2004**, *6*, 4109.

(26) Amisial, L. D.; Dai, X.; Kinney, R. A.; Krishnaswamy, A.; Warren, T. H. *Inorg. Chem.* **2004**, *43*, 6537.

(27) Harlan, E. W.; Holm, R. H. *J. Am. Chem. Soc.* **1990**, *112*, 186.

(28) Abbreviations: (a) Ts = *p*-toluenesulfonyl; (b) Et$_2$dtc = *N*,*N*-diethyldithiocarbamate; (c) Tp′ = hydridotris(3,5-dimethyl-1-pyrazolyl)borate; (d) TMP = 5,10,15,20-tetramesitylporphyrinato(2−); (e) dtbpe = 1,2-bis(di-*tert*-butylphosphino)ethane; (f) TPP = 5,10,15,20-tetraphenylporphyrinato(2−); (g) Ms = *p*-methoxybenzenesulfonyl; (h) Bs = benzenesulfonyl; (i) Cs = *p*-chlorobenzenesulfonyl; (j) Ns = *p*-nitrobenzenesulfonyl; (k) 2,6-Cl$_2$TPP = 5,10,15,20-tetrakis(2,6-dichlorophenyl)porphyrinato(2−); (l) F$_{20}$-TPP = 5,10,15,20-tetrakis(pentafluorophenyl)porphyrinato(2−); (m) TTP = 5,10,15,20-tetrakis(*p*-tolyl)porphyrinato(2−); (n) 4-Cl-TPP = 5,10,15,-20-tetrakis(*p*-chlorophenyl)porphyrinato(2−); (o) 4-OMe-TPP = 5,10,15,-20-tetrakis(*p*-methoxyphenyl)porphyrinato(2−); (p) OEP = 2,3,7,8,12,13,-17,18-octaethylporphyrinato(2−); (q) Por* = 5,10,15,20-tetrakis{(1*S*,4*R*,5*R*,8*S*)-1,2,3,4,5,6,7,8-octahydro-1,4:5,8-dimethanoanthracen-9-yl}porphyrinato(2−).

(29) Pérez, P. J.; White, P. S.; Brookhart, M.; Templeton, J. L. *Inorg. Chem.* **1994**, *33*, 6050.

(30) (a) Au, S.-M.; Fung, W.-H.; Cheng, M.-C.; Che, C.-M.; Peng, S.-M. *Chem. Commun*. **1997**, 1655. (b) Au, S.-M.; Huang, J.-S.; Yu, W.-Y.; Fung, W.-H.; Che, C.-M. *J. Am. Chem. Soc.* **1999**, *121*, 9120.

(31) Au, S.-M.; Fung, W.-H.; Huang, J.-S.; Cheung, K.-K.; Che, C.-M. *Inorg. Chem.* **1998**, *37*, 6564.

(32) Selected examples: (a) Sharpless, K. B.; Patrick, D. W.; Truesdale, L. K.; Biller, S. A. *J. Am. Chem. Soc.* **1975**, *97*, 2305. (b) Chong, A. O.; Oshima, K.; Sharpless, K. B. *J. Am. Chem. Soc.* **1977**, *99*, 3420. (c) Patrick, D. W.; Truesdale, L. K.; Biller, S. A.; Sharpless, K. B. *J. Org. Chem.* **1978**, *43*, 2628. (d) Muñiz, K.; Nieger, M.; Mansikkamäki, H. *Angew. Chem., Int. Ed.* **2003**, *42*, 5958.

(33) Groves, J. T.; Takahashi, T. *J. Am. Chem. Soc.* **1983**, *105*, 2073.

(34) Waterman, R.; Hillhouse, G. L. *J. Am. Chem. Soc.* **2003**, *125*, 13350.

(35) (a) Garrison, J. M.; Ostović, D.; Bruice, T. C. *J. Am. Chem. Soc.* **1989**, *111*, 4960. (b) Che, C.-M.; Li, C.-K.; Tang, W.-T.; Yu, W.-Y. *J. Chem. Soc., Dalton Trans.* **1992**, 3153.

(36) Bryant, J. R.; Mayer, J. M. *J. Am. Chem. Soc.* **2003**, *125*, 10351.

Scheme 1

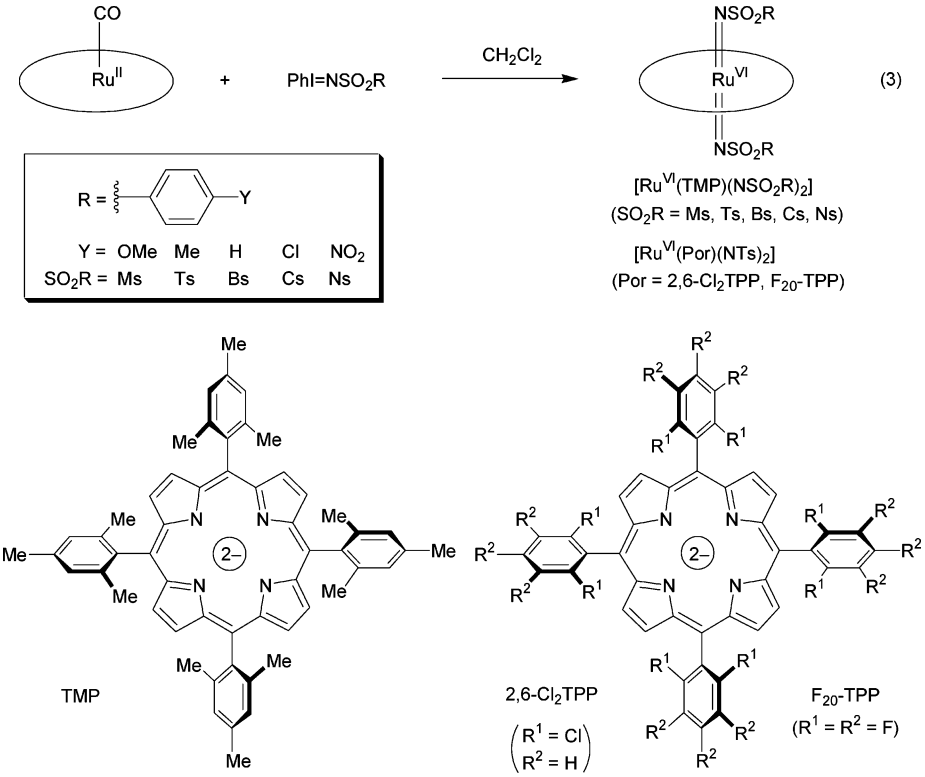

It was previously reported that the efficiency of dirhodium- or copper-catalyzed alkene aziridination with PhI=NSO_2R[5e,8a,b] and the product yields in ruthenium-, manganese-, dirhodium-, or copper-catalyzed aziridination/amidation with "$PhI(OAc)_2$ + NH_2SO_2R"[10e−g,18] or "PhIO + NH_2SO_2R", [11d−g] markedly depend on the electronic properties of the R groups. However, the origin of these observations is unclear. A possible reason is the tuning of the reactivity of the putative "M=NSO_2R" species by R groups. Therefore, examination of the effect of imido substituents on the rate constants of the alkene aziridination and C−H bond amidation by isolable metal imido complexes is of importance.

In the present work, we report the preparation of a series of $[Ru^{VI}(Por)(NSO_2R)_2]$ complexes bearing various SO_2R groups and porphyrin ligands, along with their reactivities and electrochemistry. By varying the substituent R or porphyrin ligand of $[Ru^{VI}(Por)(NSO_2R)_2]$, a tuning of the $E_{1/2}(Ru^{VI/V})$ value over a range of −0.41 to −0.12 V vs $Cp_2Fe^{+/0}$ was observed. The effect of C−H bond dissociation energies, $Ru^{VI/V}$ reduction potentials, and imido substituents on reaction rate constants, together with the relative reactivity of 3° versus 2° versus 1° C−H bonds in their amidation by $[Ru^{VI}(Por)(NSO_2R)_2]$, has been examined.

Results

Synthesis and Characterization. Scheme 1 depicts the new Ru=NSO_2R complexes prepared in this work. Reaction of $[Ru^{II}(TMP)(CO)]$ [28d] with 4 equiv of PhI=NSO_2R, wherein SO_2R = Ms,[28g] Ts,[28a] Bs,[28h] Cs,[28i] and Ns,[28j] afforded the corresponding $[Ru^{VI}(TMP)(NSO_2R)_2]$ (reaction 3 in Scheme 1). A similar reaction of $[Ru^{II}(Por)(CO)]$ for Por = 2,6-Cl_2TPP[28k] and F_{20}-TPP[28l] with PhI=NTs in CH_2Cl_2 gave $[Ru^{VI}(2,6\text{-}Cl_2TPP)(NTs)_2]$ and $[Ru^{VI}(F_{20}\text{-}TPP)(NTs)_2]$. All these imido complexes were isolated in about 70% yields.

Previous preparation of $[Ru^{VI}(Por)(NTs)_2]$ from reaction 3 led to the isolation of $[Ru^{VI}(Por)(NTs)_2]$ with Por = TPP,[30b] TTP,[28m,30b] 4-Cl-TPP,[28n,30b] 4-OMe-TPP,[28o,30b] OEP,[28p,30b] and Por*.[10f,28q] The applicability of this reaction to a wide variety of porphyrin ligands and different SO_2R groups is remarkable, which demonstrates the generality of this synthetic route to bis(arenesulfonylimido)ruthenium(VI) porphyrins.

The above $[Ru^{VI}(Por)(NSO_2R)_2]$ complexes are diamagnetic and have the following spectral features in common: (i) the mass spectra each show a prominent peak attributable to the parent ion $[M]^+$; (ii) the NMR pyrrolic proton (H_β) signals and the IR "oxidation state marker" bands[30b] are comparable to those of the corresponding $[Ru^{VI}(Por)O_2]$;[37] (iii) the axial SO_2R groups give substantially upfield shifted ^1H NMR signals compared to those in NH_2SO_2R; and (iv) the UV−vis spectra exhibit red shifted Soret and β bands compared with the corresponding $[Ru^{II}(Por)(CO)]$ counterpart.

For $[Ru^{VI}(TMP)(NSO_2R)_2]$, the H_β signals (δ = 8.67−8.71 ppm) and the β bands (535−536 nm) do not significantly vary among the R groups *p*-C_6H_4OMe, *p*-C_6H_4Me, C_6H_5, *p*-C_6H_4Cl, and *p*-$C_6H_4NO_2$. A small blue shift upon increasing electron-withdrawing strength of the R group is reflected from the Soret bands at 422, 421, 420, 419, and 416 nm for R = *p*-C_6H_4OMe, *p*-C_6H_4Me, C_6H_5, *p*-C_6H_4Cl, and *p*-$C_6H_4NO_2$, respectively. Possibly, such a blue shift arises from a decrease in π-donor strength of the imido ligand.

In the case of $[Ru^{VI}(Por)(NTs)_2]$, the H_β chemical shift increases along TMP → 2,6-Cl_2TPP → F_{20}-TPP ligands (δ = 8.67, 8.83, 9.01 ppm, respectively). The Soret and β bands of $[Ru^{VI}(2,6\text{-}Cl_2TPP)(NTs)_2]$ (422 and 534 nm) are similar to, whereas those of $[Ru^{VI}(F_{20}\text{-}TPP)(NTs)_2]$ (418 and 528 nm) are

(37) (a) Groves, J. T.; Quinn, R. *Inorg. Chem.* **1984**, *23*, 3844. (b) Leung, W.-H.; Che, C.-M. *J. Am. Chem. Soc.* **1989**, *111*, 8812. (c) Ho, C.; Leung, W.-H.; Che, C.-M. *J. Chem. Soc., Dalton Trans.* **1991**, 2933.

blue shifted from, the corresponding bands of $[Ru^{VI}(TMP)(NTs)_2]$. These phenomena are reminiscent of those observed for the $[Ru^{II}(Por)(CO)]$ counterparts.

$[Ru^{VI}(F_{20}\text{-TPP})(NTs)_2]$ exhibits almost identical ^1H NMR spectrum to that of $[Os^{VI}(F_{20}\text{-TPP})(NTs)_2]$,[38] the latter has been structurally characterized by X-ray crystallography.[38] ^{19}F NMR spectrum of $[Ru^{VI}(F_{20}\text{-TPP})(NTs)_2]$ ($\delta = -135.5, -150.7, -161.1$ ppm for the *o*-, *p*-, *m*-F of the *meso*-pentafluorophenyl groups, respectively) reveals that the two *o*-F (and *m*-F as well) of each *meso*-pentafluorophenyl group have the same chemical shift, consistent with the symmetric axial coordination in the complex.

Stability. Like previously reported $[Ru^{VI}(Por)(NTs)_2]$,[30b] the $[Ru^{VI}(Por)(NSO_2R)_2]$ prepared in this work are stable for at least several hours in highly purified CH_2Cl_2 solution at room temperature under an inert atmosphere. The stability of these imido complexes in aerobic solutions is considerably lower and increases with the electron-donating and/or sterically demanding strength of the porphyrin ligand and the electron-donating strength of the R groups. For example, in CH_2Cl_2 solution open to air at room temperature, $[Ru^{VI}(F_{20}\text{-TPP})(NTs)_2]$, $[Ru^{VI}(TPP)(NTs)_2]$, $[Ru^{VI}(TMP)(NNs)_2]$, $[Ru^{VI}(TMP)(NTs)_2]$, and $[Ru^{VI}(TMP)(NMs)_2]$ (concentrations $\approx 5 \times 10^{-4}$ M) exhibited appreciable decomposition after about 0.25, 0.5, 1.5, 3, and 3.5 h, respectively, as revealed by UV−vis spectroscopy. Attempts to isolate $[Ru^{VI}(F_{20}\text{-TPP})(NNs)_2]$ in a pure form have not been successful. This complex, which features a H_β signal ($\delta = 9.20$ ppm) and Soret and β bands (413 and 528 nm, respectively) comparable to those of $[Ru^{VI}(F_{20}\text{-TPP})(NTs)_2]$ and exhibits the parent ion cluster peak at *m*/*z* 1474, could be generated in situ from the reaction of $[Ru^{II}(F_{20}\text{-TPP})(CO)]$ with PhI═NNs in CH_2Cl_2.

Upon prolonged standing in aerobic solution, $[Ru^{VI}(TMP)(NSO_2R)_2]$ gradually converted into nitrido complexes $[Ru^{VI}(TMP)(N)(NHSO_2R)]$ (like the conversion of $[Ru^{VI}(TMP)(NTs)_2]$ to $[Ru^{VI}(TMP)(N)(NHTs)]$ [39a]), different from the formation of nitrosyl ruthenium porphyrins in an aerobic solution of $[Ru^{VI}(Por)(O)(NBu^t)]$ upon standing.[39b] For the other $[Ru^{VI}(Por)(NSO_2R)_2]$ complexes, their degradation products in aerobic solutions have not been identified yet.

Electrochemistry. The cyclic voltammograms of $[Ru^{VI}(TMP)(NSO_2R)_2]$ (SO_2R = Ms, Ts, Bs, Cs, Ns) and $[Ru^{VI}(Por)(NTs)_2]$ (Por = TPP, 2,6-Cl_2TPP, F_{20}-TPP) in CH_2Cl_2 solutions each exhibit two reversible or quasi-reversible reduction couples I and II, together with one reversible oxidation couple III; the corresponding half-wave potentials (vs $Cp_2Fe^{+/0}$) are listed in Table 1, and a typical cyclic voltammogram is depicted in Figure 2a. There are also two irreversible waves, IV and V, in each of the cyclic voltammograms. However, if the scan was reversed at the potential immediately after the cathodic wave of the first reduction (I), the irreversible wave V disappeared (Figure 2b), regardless of whether the initial scan was in the anodic or cathodic direction. It is likely that the irreversible wave V stems from the species generated by the irreversible reduction IV.

The cyclic voltammogram of $[Ru^{VI}(TMP)O_2]$ was also recorded, which is shown in Figure 2c for comparison. This complex exhibits one reversible oxidation couple similar to that of $[Ru^{VI}(TMP)(NSO_2R)_2]$. However, the reduction of $[Ru^{VI}(TMP)O_2]$ is irreversible and occurs at a potential markedly more cathodic than those of $[Ru^{VI}(TMP)(NSO_2R)_2]$.

Table 1. Half-Wave Potentials (V vs $Cp_2Fe^{+/0}$) of $[Ru^{VI}(Por)(NSO_2R)_2]$ in CH_2Cl_2 Containing 0.1 M $[NBu^n_4]PF_6$ (Scan Rate = 100 mV s^{-1})

	reduction		oxidation
complex	I	II	III
$[Ru^{VI}(TMP)(NMs)_2]$	−0.41	−1.51	0.61
$[Ru^{VI}(TMP)(NTs)_2]$	−0.38	−1.54	0.62
$[Ru^{VI}(TMP)(NBs)_2]$	−0.34	−1.58	0.67
$[Ru^{VI}(TMP)(NCs)_2]$	−0.27	−1.46	0.69
$[Ru^{VI}(TMP)(NNs)_2]$	−0.12	−1.61	0.75
$[Ru^{VI}(TPP)(NTs)_2]$	−0.27	−1.45	0.69
$[Ru^{VI}(2,6\text{-}Cl_2TPP)(NTs)_2]$	−0.34	−1.27	0.80
$[Ru^{VI}(F_{20}\text{-TPP})(NTs)_2]$	−0.12	−1.12	1.18

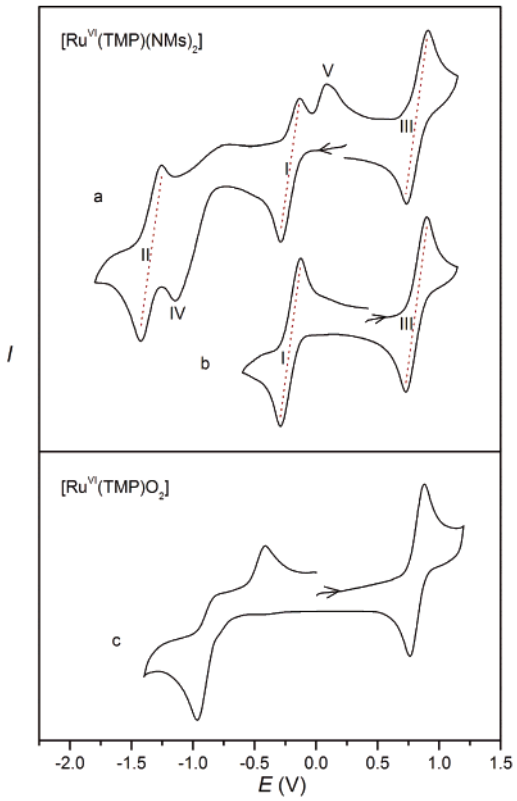

Figure 2. Cyclic voltammograms of $[Ru^{VI}(TMP)(NMs)_2]$ (a and b) and $[Ru^{VI}(TMP)O_2]$ (c) in CH_2Cl_2 at a scan rate of 100 mV s^{-1}. The potential *E* is versus 0.1 M $Ag/AgNO_3$ in MeCN.

Reactions with Hydrocarbons. (i) Product Analysis. We examined the stoichiometric reactions of $[Ru^{VI}(TMP)(NSO_2R)_2]$ (SO_2R = Ms, Ts, Bs, Cs, Ns) and $[Ru^{VI}(Por)(NTs)_2]$ (Por = 2,6-Cl_2TPP, F_{20}-TPP) with a series of hydrocarbons in CH_2Cl_2 containing pyrazole (Hpz, 2% w/w).[40] These reactions, like those of $[Ru^{VI}(TPP)(NTs)_2]$,[30b] resulted in alkene aziridination or C−H bond amidation, accompanied by formation of $[Ru^{IV}(Por)(NHSO_2R)(pz)]$ (reactions 4 and 5 in Schemes 2 and 3). Several

(38) Li, Y.; Huang, J.-S.; Zhou, Z.-Y.; Che, C.-M. *J. Am. Chem. Soc.* **2001**, *123*, 4843.
(39) (a) Leung, S. K.-Y.; Huang, J.-S.; Liang, J.-L.; Che, C.-M.; Zhou, Z.-Y. *Angew. Chem., Int. Ed.* **2003**, *42*, 340. (b) Huang, J.-S.; Sun, X.-R.; Leung, S. K.-Y.; Cheung, K.-K.; Che, C.-M. *Chem.—Eur. J.* **2000**, *6*, 334.
(40) In the presence of pyrazole, the reactions of hydrocarbons with the $[Ru^{VI}(Por)(NSO_2R)_2]$ reported in this work are simple processes, as revealed by the appearance of isosbestic points in the UV−vis spectral changes during the reactions (no isosbestic points were observed in the absence of pyrazole). Because pyrazole itself was not found to react with these imido complexes on the time scale of their reactions with hydrocarbons, its role here could be the trapping of transient intermediates generated from the attack of $[Ru^{VI}(Por)(NSO_2R)_2]$ by hydrocarbons.

Scheme 2

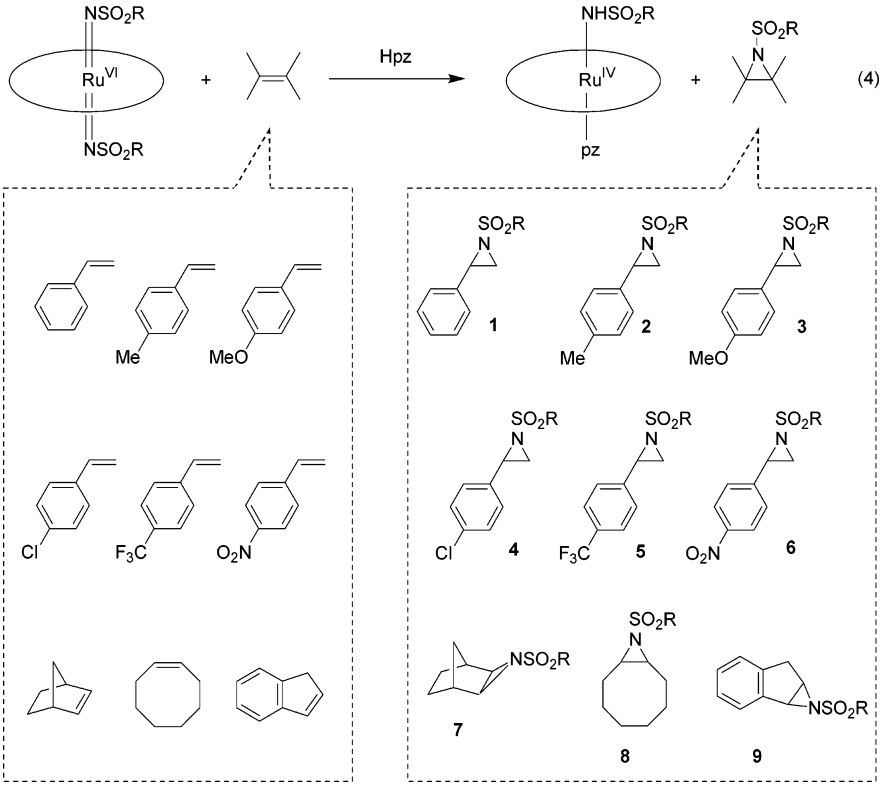

Scheme 3

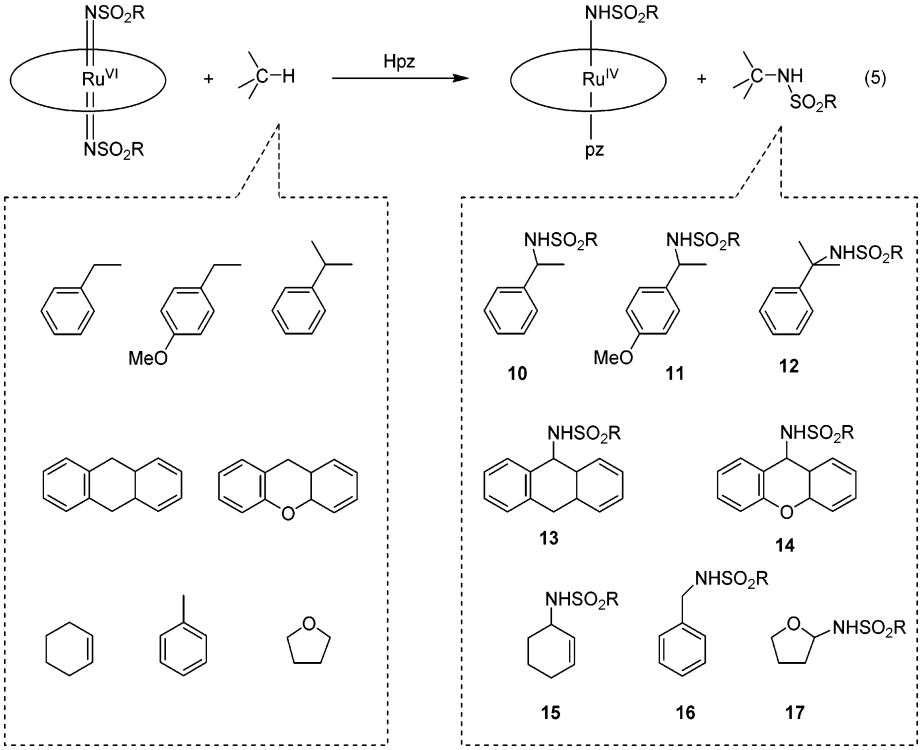

of the $[Ru^{IV}(Por)(NHSO_2R)(pz)]$ complexes, namely, $[Ru^{IV}(F_{20}$-TPP)(NHTs)(pz)] and $[Ru^{IV}(TMP)(NHSO_2R)(pz)]$ (SO_2R = Ms, Cs, Ns), were isolated, and the structure of $[Ru^{IV}(TMP)(NHCs)$-(pz)] was determined by X-ray crystallography (see Table 2 and Figure 3).

An interesting feature in the structure of $[Ru^{IV}(TMP)(NHCs)$-(pz)] is the large dihedral angle between the axial phenyl plane and the porphyrin plane (about 55°), probably resulting from a steric interaction between the amido phenyl group and the porphyrin *meso*-mesityl groups (see the space-filling structure in the upper right corner of Figure 3). In previously reported crystal structures of $[Ru^{IV}(Por)(NHTs)(pz)]$ (Por = TPP,[30a] OEP [30b]) and $[Os^{VI}(Por)(NTs)_2]$ (Por = TPP,[31] F_{20}-TPP[38]) bearing sterically unencumbered porphyrin ligands, such planes are

Table 2. Crystal Data and Structure Refinement for $[Ru^{IV}(TMP)(NHCs)(pz)]\cdot 5H_2O$

formula	$C_{65}H_{60}ClN_7O_2SRu\cdot 5H_2O$
Mr	1229.87
crystal system	monoclinic
space group	$P2_1/n$
a, Å	18.363(4)
b, Å	19.578(4)
c, Å	19.987(4)
α, deg	90
β, deg	113.78(3)
γ, deg	90
F(000)	2568
V, Å^3	6575(2)
Z	4
ρ_{calc}, Mg m^{-3}	1.243
μ(Mo Kα), mm^{-1}	0.365
θ range, deg	1.27−25.23
reflections collected	14635
independent reflections	5801
parameters	384
final *R* indices ($I > 2\sigma(I)$)	$R1 = 0.09$, $wR2 = 0.24$
goodness-of-fit	0.98
largest diff. peak/hole, e Å^{-3}	0.824/−0.689

almost parallel to each other (possibly due to $\pi-\pi$ interactions). The Ru−N(NHSO$_2$R) distance (2.00(1) Å), N(NHSO$_2$R)−Ru−N(pz) angle (172.4(4)°), and S−N−Ru angle (138.6(7)°) in $[Ru^{IV}(TMP)(NHCs)(pz)]$ are comparable to those in $[Ru^{IV}(TPP)(NHTs)(pz)]$ (2.025(11) Å, 176.2(4)°, 136.4(7)°)[30a] and $[Ru^{IV}(OEP)(NHTs)(pz)]$ (2.020(6) Å, 173.1(2)°, 135.6(3)°).[30b]

After reaction with $[Ru^{VI}(TMP)(NSO_2R)_2]$, the alkenes *p*-XC$_6$H$_4$CH=CH$_2$ (X = H, Me, OMe, Cl, CF$_3$, NO$_2$), norbornene, *cis*-cyclooctene, and indene were converted into the corresponding aziridines **1**−**9** in 68−85% yields (Scheme 2 and entries 1−15 in Table 3), whereas ethylbenzenes *p*-XC$_6$H$_4$CH$_2$-CH$_3$ (X = H, OMe), cumene, 9,10-dihydroanthracene, xanthene, cyclohexene, and toluene were converted into the corresponding amides **10**−**16** in 22−82% yields (Scheme 3 and entries 16−28 in Table 3). In almost all cases, the main byproduct was NH$_2$SO$_2$R (SO$_2$R = Ms, Ts, Bs, Cs, or Ns, depending on the

Table 3. Stoichiometric Imido Transfer Reactions of $[Ru^{VI}(Por)(NSO_2R)_2]$ with Hydrocarbons in CH_2Cl_2 Containing Pyrazole (2% w/w) at 298 K

	$[Ru^{VI}(Por)(NSO_2R)_2]$				yield
entry	Por	SO$_2$R	substrate	product	(%)
1	TMP	Ms	styrene	**1**	73
2	TMP	Ts	styrene	**1**	77
3	TMP	Bs	styrene	**1**	72
4	TMP	Cs	styrene	**1**	75
5	TMP	Ns	styrene	**1**	82
6	2,6-Cl$_2$TPP	Ts	styrene	**1**	72
7	F$_{20}$-TPP	Ts	styrene	**1**	78
8	TMP	Ns	*p*-methylstyrene	**2**	83
9	TMP	Ns	*p*-methoxystyrene	**3**	85
10	TMP	Ns	*p*-chlorostyrene	**4**	80
11	TMP	Ns	*p*-trifluoromethylstyrene	**5**	83
12	TMP	Ns	*p*-nitrostyrene	**6**	80
13	TMP	Ns	norbornene	**7**	78
14	TMP	Ns	*cis*-cyclooctene	**8**	75
15	TMP	Ns	indene	**9**	68
16	TMP	Ms	ethylbenzene	**10**	71
17	TMP	Ts	ethylbenzene	**10**	72
18	TMP	Bs	ethylbenzene	**10**	70
19	TMP	Cs	ethylbenzene	**10**	72
20	TMP	Ns	ethylbenzene	**10**	75
21	2,6-Cl$_2$TPP	Ts	ethylbenzene	**10**	70
22	F$_{20}$-TPP	Ts	ethylbenzene	**10**	71
23	TMP	Ns	*p*-methoxyethylbenzene	**11**	75
24	TMP	Ns	cumene	**12**	73
25	TMP	Ns	9,10-dihydroanthracene	**13**	65
26	TMP	Ns	xanthene	**14**	82
27	TMP	Ns	cyclohexene	**15**	75
28	TMP	Ns	toluene	**16**	22
29	TPP	Ts	tetrahydrofuran	**17**	40
30	TMP	Ts	tetrahydrofuran	**17**	53
31	2,6-Cl$_2$TPP	Ts	tetrahydrofuran	**17**	68

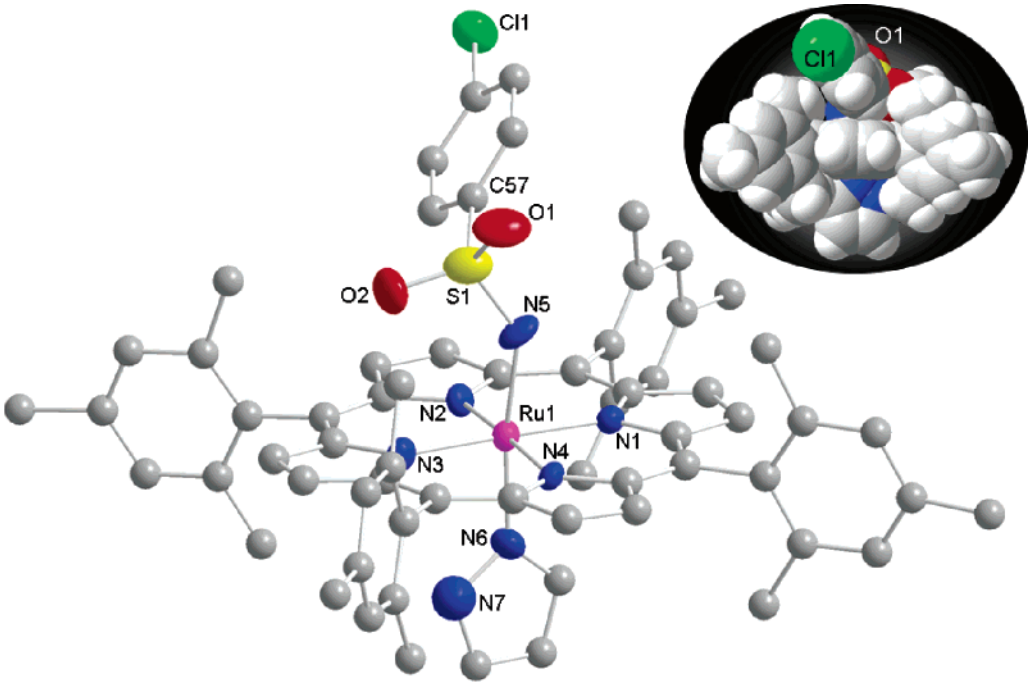

Figure 3. Structure of $[Ru^{IV}(TMP)(NHCs)(pz)]$ with omission of hydrogen atoms (thermal ellipsoid probability level: 30%). A space-filling representation of the structure (with hydrogen atoms) viewed along the N2···N4 axis is shown in the upper right corner. Selected bond distances (Å): Ru1−N1 2.037(9), Ru1−N2 2.034(9), Ru1−N3 2.042(9), Ru1−N4 2.010(9), Ru1−N5 2.00(1), Ru1−N6 2.07(1), N5−S1 1.57(1), C57−S1 1.78(2), S1−O1 1.443(9), S1−O2 1.462(9). Selected bond angles (deg): N5−Ru1−N6 172.4(4), S1−N5−Ru1 138.6(7), C57−S1−N5 104.3(7).

imido complex), with the total yield of the aziridine/amide and NH_2SO_2R close to 100%.

We also examined the reaction of $[Ru^{VI}(Por)(NTs)_2]$ (Por = TPP, TMP, 2,6-Cl_2TPP) with tetrahydrofuran, which afforded the amidation product **17** (Scheme 3) in 40−68% yields (entries 29−31, Table 3). Amidation of tetrahydrofuran with PhI=NTs catalyzed by $[Ru^{II}(Por)(CO)]$ to give **17** has been reported,[10d] but no corresponding amidation of this substrate by a well characterized metal imido complex has previously been known.

(ii) Kinetic Studies. The reactions of $[Ru^{VI}(TMP)(NSO_2R)_2]$ (SO_2R = Ms, Ts, Bs, Cs, Ns) and $[Ru^{VI}(Por)(NTs)_2]$ (Por = 2,6-Cl_2TPP, F_{20}-TPP) with hydrocarbons in CH_2Cl_2 solution containing pyrazole (2% w/w) were monitored by UV−vis spectrophotometry under the conditions similar to those reported for $[Ru^{VI}(TPP)(NTs)_2]$.[30b] In general, isosbestic UV−vis spectral changes have been observed (see, for example, Figures S1−S5 in Supporting Information), with the final spectra essentially identical to those of $[Ru^{IV}(Por)(NHSO_2R)(pz)]$. Control experiments revealed no appreciable reaction of the imido complexes with pyrazole on the time scale of the kinetic studies.

Pseudo-first-order rate constants, k_{obs}, were determined by the method described in previous work.[30b] The k_{obs} values correlate linearly with the hydrocarbon concentrations (see, for example, Figures S6−S9 in Supporting Information). From the k_{obs} versus hydrocarbon concentration plots, the second-order rate constants, k_2, were determined and listed in Table 4.

Table 4. Second-Order Rate Constants (k_2) for Imido Transfer Reactions of $[Ru^{VI}(Por)(NSO_2R)_2]$ with Hydrocarbons in CH_2Cl_2 Containing Pyrazole (2% w/w) at 298 K

entry	$[Ru^{VI}(Por)(NSO_2R)_2]$ Por	SO_2R	substrate	$k_2 \times 10^3$ ($dm^3\ mol^{-1}\ s^{-1}$)
1	TMP	Ms	styrene	1.47 ± 0.07
2	TMP	Ts	styrene	3.0 ± 0.2
3	TMP	Bs	styrene	4.2 ± 0.2
4	TMP	Cs	styrene	11.5 ± 0.6
5	TMP	Ns	styrene	83 ± 4
6	2,6-Cl_2TPP	Ts	styrene	4.4 ± 0.2
7	F_{20}-TPP	Ts	styrene	56 ± 3
8	TPP	Ts	styrene	9.0 ± 0.1[a]
9	TMP	Ns	*p*-methylstyrene	141 ± 5
10	TMP	Ns	*p*-methoxystyrene	1520 ± 70
11	TMP	Ns	*p*-fluorostyrene	105 ± 5
12	TMP	Ns	*p*-chlorostyrene	69 ± 3
13	TMP	Ns	*p*-trifluoromethylstyrene	9.7 ± 0.5
14	TMP	Ns	*p*-nitrostyrene	7.2 ± 0.3
15	TMP	Ns	norbornene	1.26 ± 0.06
16	TMP	Ns	*cis*-cyclooctene	1.32 ± 0.07
17	TMP	Ns	indene	27 ± 2
18	TMP	Ms	ethylbenzene	0.30 ± 0.02
19	TMP	Ts	ethylbenzene	0.33 ± 0.02
20	TMP	Bs	ethylbenzene	0.53 ± 0.03
21	TMP	Cs	ethylbenzene	0.61 ± 0.03
22	TMP	Ns	ethylbenzene	2.4 ± 0.1
23	TMP	Ns	ethylbenzene-d_{10}	0.50 ± 0.02
24	2,6-Cl_2TPP	Ts	ethylbenzene	0.57 ± 0.03
25	F_{20}-TPP	Ts	ethylbenzene	13.8 ± 0.7
26	TPP	Ts	ethylbenzene	3.60 ± 0.07[a]
27	TMP	Ns	*p*-methoxyethylbenzene	19.7 ± 0.9
28	TMP	Ms	cumene	0.029 ± 0.002
29	TMP	Ts	cumene	0.032 ± 0.001
30	TMP	Bs	cumene	0.048 ± 0.002
31	TMP	Cs	cumene	0.074 ± 0.003
32	TMP	Ns	cumene	0.25 ± 0.01
33	F_{20}-TPP	Ts	cumene	10.9 ± 0.5
34	TPP	Ts	cumene	1.5 ± 0.1[a]
35	TMP	Ns	9,10-dihydroanthracene	130 ± 6
36	F_{20}-TPP	Ts	9,10-dihydroanthracene	600 ± 30
37	TMP	Ns	xanthene	8100 ± 400
38	TMP	Ns	*p*-nitroethylbenzene	0.96 ± 0.05
39	F_{20}-TPP	Ts	xanthene	14400 ± 600
40	TMP	Ns	fluorene	64 ± 3
41	F_{20}-TPP	Ts	fluorene	104 ± 4
42	TMP	Ns	cyclohexene	13.6 ± 0.8
43	F_{20}-TPP	Ts	cyclohexene	48 ± 2
44	TMP	Ms	toluene	0.026 ± 0.001
45	TMP	Ts	toluene	0.046 ± 0.002
46	TMP	Bs	toluene	0.074 ± 0.003
47	TMP	Cs	toluene	0.15 ± 0.01
48	TMP	Ns	toluene	0.93 ± 0.04
49	2,6-Cl_2TPP	Ts	toluene	0.13 ± 0.01
50	F_{20}-TPP	Ts	toluene	7.1 ± 0.3
51	TPP	Ts	toluene	0.48 ± 0.02
52	TMP	Ms	tetrahydrofuran	0.56 ± 0.02
53	TMP	Ts	tetrahydrofuran	0.86 ± 0.04
54	TMP	Bs	tetrahydrofuran	1.50 ± 0.08
55	TMP	Cs	tetrahydrofuran	2.30 ± 0.09
56	TMP	Ns	tetrahydrofuran	10.3 ± 0.5
57	2,6-Cl_2TPP	Ts	tetrahydrofuran	1.8 ± 0.1
58	TPP	Ts	tetrahydrofuran	20 ± 1

[a] From ref 30b.

Discussion

Metal imido complexes are important metal−ligand multiply bonded species known in the literature.[41] Despite the extensive studies on their chemistry,[41] only a few types of these compounds have been found to react with hydrocarbons to afford aziridines, amines, or amides (see Introduction), a reactivity analogous to the extensively investigated oxo transfer reactions of metal oxo complexes.[42] The present work provides a number of new metal imido complexes that are reactive toward alkene aziridination and C−H bond amidation reactions, of which $[Ru^{VI}(TMP)(NSO_2R)_2]$ with SO_2R = Ms, Ts, Bs, Cs, and Ns bearing *p*-OMe, -Me, -H, -Cl, and -NO_2 substituents, respectively, constitute a unique series of well-defined metal imido complexes suitable for examining the various factors governing imido transfer reactions. Prior to this work, the imido groups in the well characterized $M{=}NSO_2R$ complexes[27,29−31] are exclusively NTs; in the cases of other metal imido complexes,[32−34] the examples with *para*-substituted imido ligands that are reactive toward hydrocarbons remain unreported.

Redox Behavior of $[Ru^{VI}(Por)(NSO_2R)_2]$. Under electrochemical conditions, $[Ru^{VI}(TMP)(NSO_2R)_2]$ with SO_2R = Ms, Ts, Bs, Cs, and Ns undergo oxidation at $E_{1/2}$ = 0.61−0.75 V vs $Cp_2Fe^{+/0}$ (Table 1). The potentials of this reversible oxidation couple are comparable to that of the oxidation of $[Ru^{VI}(TMP)O_2]$ (Figure 2c, $E_{1/2}$ = 0.69 V vs $Cp_2Fe^{+/0}$), revealing a porphyrin-centered oxidation.[43] In accord with this assignment, the oxidation potentials of $[Ru^{VI}(Por)(NTs)_2]$ for Por = TMP, TPP, 2,6-Cl_2TPP, and F_{20}-TPP ($E_{1/2}$ = 0.62−1.18 V, Table 1) increase with the electron-withdrawing strength of peripheral substituent on the porphyrin ligands. As expected, oxidation of the electron-deficient F_{20}-TPP ligand occurs at a markedly more anodic potential.

The first reduction couple of $[Ru^{VI}(Por)(NSO_2R)_2]$ has $E_{1/2}$ values in the range of −0.41 to −0.12 V vs $Cp_2Fe^{+/0}$ (Table 1), which markedly depend on the R groups and are much more anodic than those of the porphyrin-centered reduction.[44] We assign this reduction to the following electrode reaction:

$$[Ru^{VI}(Por)(NSO_2R)_2] \underset{-e}{\overset{+e}{\rightleftharpoons}} [Ru^{V}(Por)(NSO_2R)_2]^-$$

The *reversible* $Ru^{VI/V}$ reduction of $[Ru^{VI}(Por)(NSO_2R)_2]$ contrasts with the *irreversible* $Ru^{VI/V}$ reduction at $E_{p,c}$ = −1.05 V

Scheme 4

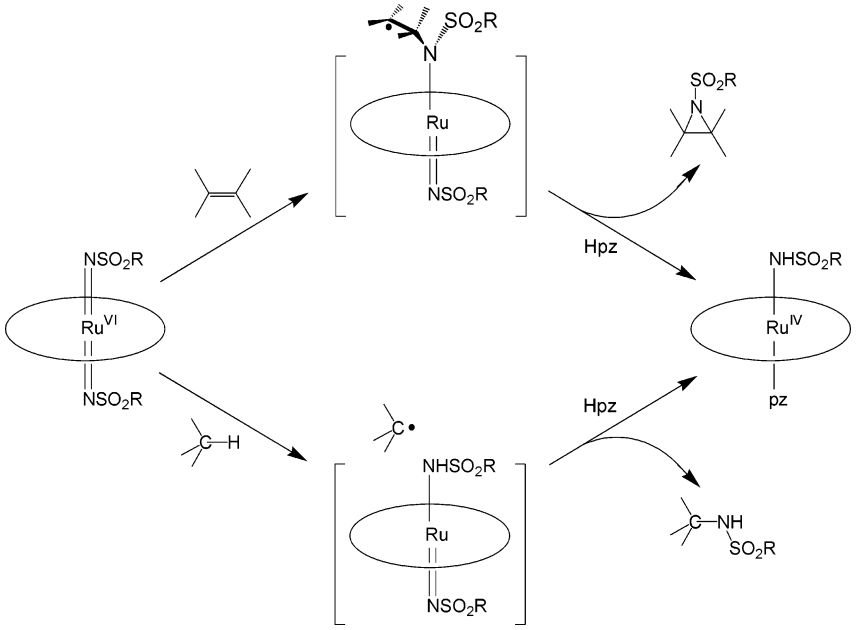

vs $Cp_2Fe^{+/0}$ observed for $[Ru^{VI}(TMP)O_2]$ (see Figure 2c), suggesting that $[Ru^{V}(Por)(NSO_2R)_2]^-$ is more stable than the respective $[Ru^{V}(Por)O_2]^-$ under the electrochemical conditions.

The reduction couple with $E_{1/2} = -1.12$ to -1.61 V vs $Cp_2Fe^{+/0}$ for $[Ru^{VI}(Por)(NSO_2R)_2]$ (Table 1) should be attributed to a porphyrin-centered reduction. Indeed, in the case of $[Ru^{VI}(Por)(NTs)_2]$ (Por = TMP, TPP, 2,6-Cl_2TPP, F_{20}-TPP), the potentials of this reduction couple increase with the electron-withdrawing strength of peripheral substituent on the porphyrin ligands, like those of the porphyrin-centered oxidation.

It can be seen from Table 1 that the $E_{1/2}(Ru^{VI/V})$ of $[Ru^{VI}(TMP)(NSO_2R)_2]$ increases with the electron-withdrawing strength of the R substituent. The electron-donating or -withdrawing property of the R group would affect the π-donor strength of imido group and thus the $E_{1/2}(Ru^{VI/V})$ value. In this work, we found that for a given porphyrin ligand, such as TMP, the $E_{1/2}(Ru^{VI/V})$ could be tuned by about 300 mV when the R group changes from *p*-C_6H_4OMe to *p*-$C_6H_4NO_2$.

Changing the porphyrin ligand also affects the $E_{1/2}$ of $Ru^{VI/V}$ couple, as reflected by the data in Table 1. The more anodic $E_{1/2}(Ru^{VI/V})$ of $[Ru^{VI}(F_{20}\text{-TPP})(NTs)_2]$ is consistent with the electron-deficient nature of the F_{20}-TPP (compared with the other porphyrin ligands). The more cathodic $E_{1/2}(Ru^{VI/V})$ of $[Ru^{VI}(2,6\text{-}Cl_2TPP)(NTs)_2]$ than that of $[Ru^{VI}(TPP)(NTs)_2]$ seems unusual, which cannot be clearly rationalized yet. A possible reason is that the *meso*-aryl rings in 2,6-Cl_2TPP are perpendicular to the porphyrin ring, whereas the nonsubstituted *meso*-phenyl rings and the porphyrin ring in TPP are more in plane and thus more in resonance. By altering porphyrin ligands among TMP, TPP, 2,6-Cl_2TPP, and F_{20}-TPP, a change of up to 260 mV in $E_{1/2}(Ru^{VI/V})$ was observed.

Combining the above dependence of $E_{1/2}(Ru^{VI/V})$ on imido substituents and porphyrin ligands, one would expect that there could be an overall tuning of the $E_{1/2}(Ru^{VI/V})$ of $[Ru^{VI}(Por)(NSO_2R)_2]$ by about 560 mV through changing both the imido groups and porphyrin ligands.

The $Ru^{VI/V}$ reduction of $[Ru^{VI}(TMP)(NSO_2R)_2]$ occurs at a more anodic potential than that of $[Ru^{VI}(TMP)O_2]$ (cf. Figure 2b,c), indicating that the Ru^{VI} ion in the arenesulfonylimido complexes is more electron-deficient than that in the dioxo counterpart.

Effects of Imido Substituents, C−H Bond Dissociation Energies, and $Ru^{VI/V}$ Reduction Potentials on k_2 for Alkene Aziridination or C−H Bond Amidation by $[Ru^{VI}(Por)(NSO_2R)_2]$. We propose that the imido transfer reactions of $[Ru^{VI}(Por)(NSO_2R)_2]$ with alkenes or C−H bonds proceed by a mechanism as shown in Scheme 4, which is based on the previous mechanistic studies using $[Ru^{VI}(TPP)(NTs)_2]$.[30b] Indeed, the substituent effect on the rate constants for the reaction of *para*-substituted styrenes with $[Ru^{VI}(TMP)(NNs)_2]$ is similar to that with $[Ru^{VI}(TPP)(NTs)_2]$, as is evident from the comparable ρ^+ values of the log k_{rel} versus σ_p^+ plot for $[Ru^{VI}(TPP)(NTs)_2]$ ($\rho^+ = -1.1$)[30b] and $[Ru^{VI}(TMP)(NNs)_2]$ ($\rho^+ = -1.4$, Figure S10) and from the similar linearity of log k_{rel} versus (σ_{mb}, $\sigma_{JJ}^{\bullet}$) plots,[45] where $\sigma_{JJ}^{\bullet}$ is a radical constant, in both cases (see ref 30b and Figure S11). The kinetic isotope effect for the amidation of ethylbenzene by $[Ru^{VI}(TMP)(NNs)_2]$ ($k_H/k_D = 4.8$, cf. entries 22 and 23 in Table 4) is comparable to that for the amidation of hydrocarbons by $[Ru^{VI}(TPP)(NTs)_2]$ ($k_H/k_D = 6.1-11$).[30b]

Inspection of the results in Tables 1 and 4 reveals the following effects on the k_2 of the imido transfer reactions.

(41) For reviews, see: (a) Nugent, W. A.; Haymore, B. L. *Coord. Chem. Rev.* **1980**, *31*, 123. (b) Nugent, W. A.; Mayer, J. M. *Metal−Ligand Multiple Bonds*; Wiley-Interscience: New York, 1988. (c) Wigley, D. E. *Prog. Inorg. Chem.* **1994**, *42*, 239. (d) Eikey, R. A.; Abu-Omar, M. M. *Coord. Chem. Rev.* **2003**, *243*, 83.

(42) Selected examples: (a) Samsel, E. G.; Srinivasan, K.; Kochi, J. K. *J. Am. Chem. Soc.* **1985**, *107*, 7606. (b) Groves, J. T.; Watanabe, Y. *J. Am. Chem. Soc.* **1986**, *108*, 507. (c) Groves, J. T.; Stern, M. K. *J. Am. Chem. Soc.* **1988**, *110*, 8628. (d) Garrison, J. M.; Bruice, T. C. *J. Am. Chem. Soc.* **1989**, *111*, 191. (e) Arasasingham, R. D.; He, G.-X.; Bruice, T. C. *J. Am. Chem. Soc.* **1993**, *115*, 7985. (f) Khenkin, A. M.; Hill, C. L. *J. Am. Chem. Soc.* **1993**, *115*, 8178. (g) Stultz, L. K.; Binstead, R. A.; Reynolds, M. S.; Meyer, T. J. *J. Am. Chem. Soc.* **1995**, *117*, 2520. (h) Kaizer, J.; Klinker, E. J.; Oh, N. Y.; Rohde, J.-U.; Song, W. J.; Stubna, A.; Kim, J.; Münck, E.; Nam, W.; Que, L., Jr. *J. Am. Chem. Soc.* **2004**, *126*, 472.

(43) Chen, C.-Y.; Cheng, S.-H.; Su, Y. O. *J. Electroanal. Chem.* **2000**, *487*, 51.

(44) Li, Y.; Huang, J.-S.; Xu, G.-B.; Zhu, N.; Zhou, Z.-Y.; Che, C.-M.; Wong, K.-Y. *Chem.—Eur. J.* **2004**, *10*, 3486.

(45) Jiang, X.-K. *Acc. Chem. Res.* **1997**, *30*, 283.

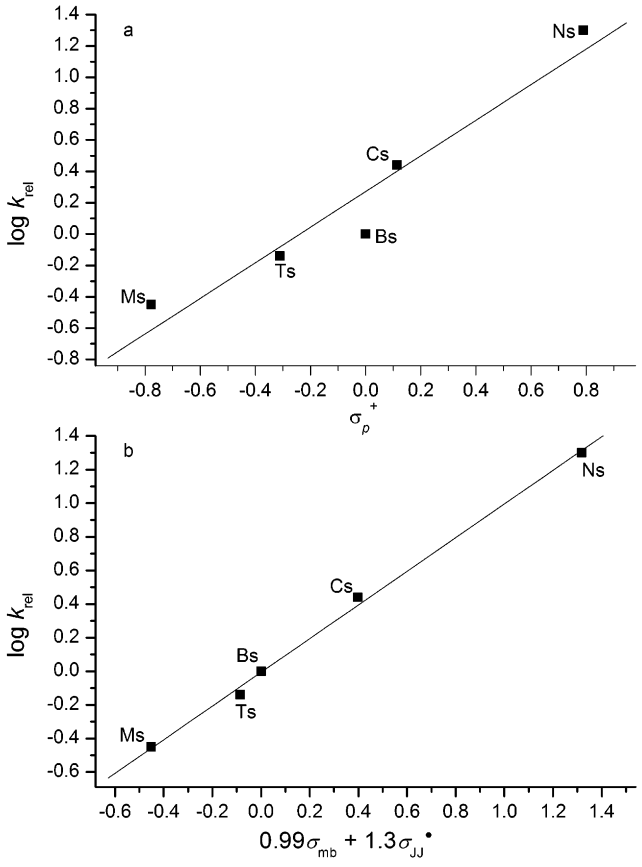

Figure 4. Plots of (a) log k_{rel} versus σ_p^+ and (b) log k_{rel} versus (σ_{mb}, $\sigma_{JJ}^{\bullet}$) at 298 K for aziridination of styrene by [Ru^{VI}(TMP)(NSO_2R)$_2$].

(i) Effect of Imido Substituents. For the reactions of [Ru^{VI}(TMP)(NSO_2R)$_2$] with styrene, the k_2 values are in the SO_2R order

$$Ms < Ts < Bs < Cs < Ns$$

(cf. entries 1−5 in Table 4), and on going from SO_2R = Ms to Ns, the reaction becomes about 56 times faster. This is remarkable considering the relatively remote location of the OMe/NO_2 groups of Ms/Ns from the reaction site. The increase in k_2 with the electron-withdrawing strength of the imido substituents reflects the electrophilic nature of the imido groups, in agreement with the electrophilicity of such groups reflected by the negative ρ^+ value of the log k_{rel} versus σ_p^+ plot for the imido transfer from [Ru^{VI}(TPP)(NTs)$_2$] or [Ru^{VI}(TMP)(NNs)$_2$] to *para*-substituted styrenes.

A linear correlation was observed between log k_{rel} and the σ_p^+ of the *para*-substituents of the imido groups (Figure 4a, ρ^+ = 1.1). Plotting log k_{rel} against (σ_{mb}, $\sigma_{JJ}^{\bullet}$) results in a much better linearity than against σ_p^+ (Figure 4b, ρ_{mb} = 0.99, $\rho_{JJ}^{\bullet}$ = 1.3). This seems to provide additional support for the rate-limiting formation of a radical intermediate in the reaction.[45] However, it remains unclear how the *para*-substituents of the imido groups interact with the radical center.

For the reactions of [Ru^{VI}(TMP)(NSO_2R)$_2$] with ethylbenzene, cumene, toluene, and tetrahydrofuran, the k_2 also increases with the electron-withdrawing strength of the R groups (cf. entries 18−22, 28−32, 44−48, and 52−56 in Table 4), but the rate increase from SO_2R = Ms to Ns in these cases is smaller, with k_2(Ns)/k_2(Ms) ≈ up to 36.

The higher reactivity of [Ru^{VI}(TMP)(NNs)$_2$] than that of [Ru^{VI}(TMP)(NSO_2R)$_2$] with the other R groups toward aziridination of styrene correlates with the higher efficiency of copper-catalyzed aziridination of alkenes with PhI=NNs than with other PhI=NSO_2R nitrogen sources.[5e,8a,b]

(ii) Effect of C−H Bond Dissociation Energies (BDEs). Mayer and co-worker established that C−H bond oxidation by metal oxo complexes involving a H-atom abstraction mechanism exhibits linear correlation between log k' (k' is the k_2 value divided by the number of reactive hydrogens) and BDE.[36] In this work, the C−H bond amidation by [Ru^{VI}(F_{20}-TPP)(NTs)$_2$] features k' values in the order

xanthene > 9,10-dihydroanthracene > fluorene > cyclohexene > cumene > ethylbenzene > toluene

similar to the case of C−H bond oxidation by metal oxo complexes.[36] There is also a linear correlation between log k' and BDE (Figure 5). This supports the H-atom abstraction mechanism proposed previously.[30b]

The larger k' for cumene (3° C−H) than for ethylbenzene (2° C−H) (k'(3° C−H)/k'(2° C−H) = 1.6) in the C−H bond amidation by [Ru^{VI}(F_{20}-TPP)(NTs)$_2$] should be noted. Previous work[30b] showed that the amidation by [Ru^{VI}(TPP)(NTs)$_2$] (k'(3° C−H)/k'(2° C−H) = 0.84) reverses the thermodynamic reactivity order cumene > ethylbenzene, opposite to the C−H bond oxidation by [Ru^{VI}(TPP)O_2] (k'(3° C−H)/k'(2° C−H) = 2.9).[37c] As depicted in Table 4, the C−H bond amidation by [Ru^{VI}(F_{20}-TPP)(NTs)$_2$] is faster than by [Ru^{VI}(TPP)(NTs)$_2$].

Remarkably, [Ru^{VI}(TMP)(NNs)$_2$], which is less reactive than [Ru^{VI}(TPP)(NTs)$_2$] and bears a sterically demanding TMP ligand, gives a k'(3° C−H)/k'(2° C−H) value of 0.2 for cumene and ethylbenzene, and the k' for cumene is even smaller than for toluene (1° C−H) (k'(3° C−H)/k'(1° C−H) = 0.8). Except for the unusually small k' value for cumene, there is a linear correlation between log k' and BDE for the C−H bond amidation by [Ru^{VI}(TMP)(NNs)$_2$] (Figure 5).

(iii) Effect of $Ru^{VI/V}$ Reduction Potentials. From the $E_{1/2}$($Ru^{VI/V}$) values of [Ru^{VI}(TMP)(NSO_2R)$_2$] (SO_2R = Ms, Ts, Bs, Cs, Ns) and the k_2 values for the reactions of these complexes with styrene, the increase in $E_{1/2}$($Ru^{VI/V}$) correlates with the increase in k_2 values. The reaction of styrene with [Ru^{VI}(TPP)O_2] gave a smaller k_2 value ($(4.3 \pm 0.3) \times 10^3$)[37c] than with [$Ru^{VI}$(TPP)($NTs$)$_2$] ($k_2 = (9.0 \pm 0.1) \times 10^3$),[30b] in accordance with the more cathodic $Ru^{VI/V}$ reduction potential of the former.

In a previous work,[30b] we reported that, for the reaction of [Ru^{VI}(TPP)(NTs)$_2$] with various alkenes, the plot of log k_2 versus the $E_{1/2}$ values of the 1e oxidation potentials of alkenes exhibits a good linearity with a slope of −1.7 V^{-1}, corresponding to a slope of α = 0.1 in the conventional Bronsted plot (log k_2 vs log K_{eq}).[30b]

The present work allows examination of the effect of driving force on the rate constants of imido transfer to a given hydrocarbon. There is a linear correlation between log k_2 and $E_{1/2}$($Ru^{VI/V}$) for the reactions of styrene with [Ru^{VI}(TMP)(NSO_2R)$_2$] (Figure 6a). The slope of the log k_2 versus $E_{1/2}$ plot is 5.9 V^{-1}, corresponding to a slope of α = 0.35 in the conventional Bronsted plot. In contrast, the epoxidation of styrene or norbornene by metal oxo complexes features log k_2 versus $E_{1/2}$ plots with larger slopes of 9−14 V^{-1}.[35]

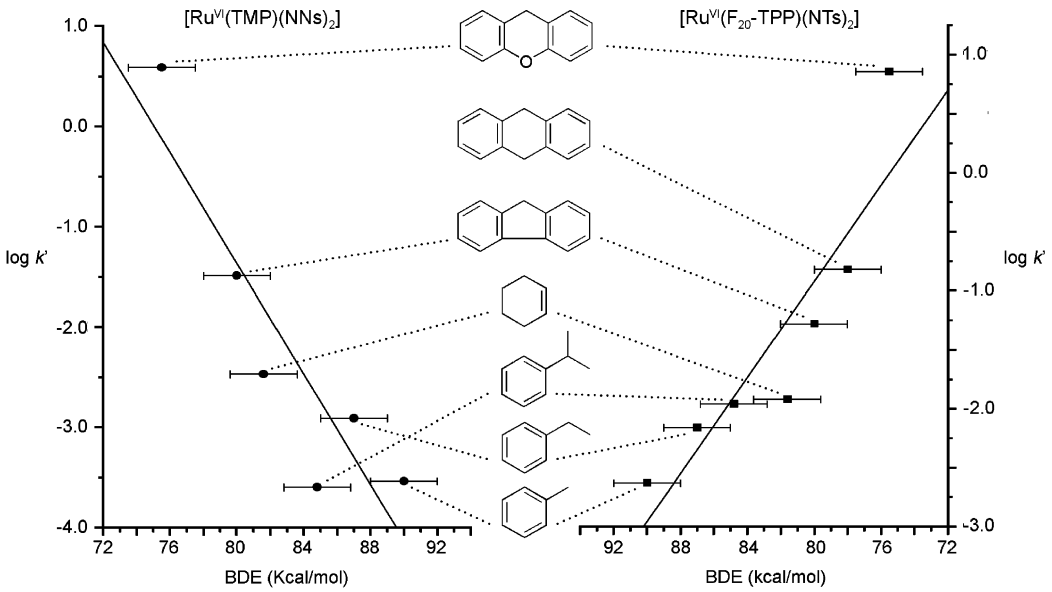

Figure 5. Plots of log k' versus BDE for reactions of $[Ru^{VI}(TMP)(NNs)_2]$ and $[Ru^{VI}(F_{20}\text{-}TPP)(NTs)_2]$ with hydrocarbons.

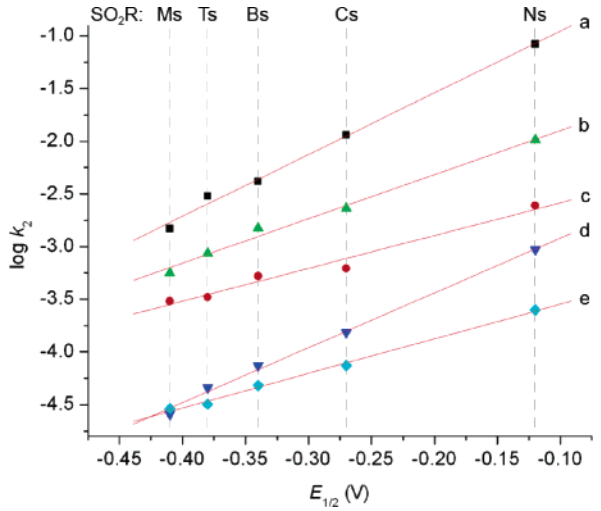

Figure 6. Plots of log k_2 versus $E_{1/2}(Ru^{VI/V})$ for reactions of $[Ru^{VI}(TMP)(NSO_2R)_2]$ with (a) styrene, (b) tetrahydrofuran, (c) ethylbenzene, (d) toluene, and (e) cumene.

The different α values obtained for the reactions of $[Ru^{VI}(TPP)(NTs)_2]$ with various alkenes[30b] and for the reactions of styrene with different $[Ru^{VI}(TMP)(NSO_2R)_2]$ suggest the presence of perpendicular contribution to the overall slope α, which approximately follows the equation[35a]

$$\alpha = \chi \pm 0.5(\tau - 1)$$

where χ is the progress of the reaction along the reaction coordinate, and τ is the "tightness" of the transition state. Through this equation and from the above two α values, we estimated the χ and τ values to be 0.225 and 0.75, respectively, which might imply that the transition state of the imido transfer reaction is earlier and more "tight" than that of the oxo transfer reaction of $[Cr^{V}(Por)O]^{+}$ with alkenes ($\chi = 0.37$, $\tau = 0.63$).[35a]

For amidation of cumene, ethylbenzene, tetrahydrofuran, or toluene by different $[Ru^{VI}(TMP)(NSO_2R)_2]$, the log k_2 versus $E_{1/2}(Ru^{VI/V})$ plots (Figure 6b−e) also exhibit a good linearity, with slopes of 3.3, 3.1, 4.2, and 5.2 V^{-1}, respectively, comparable to the slope of 5.9 V^{-1} for the reaction of styrene with $[Ru^{VI}(TMP)(NSO_2R)_2]$ (Figure 6a).

Reactions of $[Ru^{VI}(Por)(NTs)_2]$ (Por = TMP, 2,6-Cl_2TPP, TPP, F_{20}-TPP) with styrene, cumene, ethylbenzene, tetrahydrofuran, or toluene have k_2 values in the order

$$TMP < 2,6\text{-}Cl_2TPP < TPP < F_{20}\text{-}TPP$$

This is in agreement with the $E_{1/2}(Ru^{VI/V})$ of $[Ru^{VI}(Por)(NTs)_2]$, which increases along TMP → 2,6-Cl_2TPP → TPP → F_{20}-TPP (Table 1). Notably, on going from TMP to F_{20}-TPP, the reaction of $[Ru^{VI}(Por)(NTs)_2]$ with styrene and ethylbenzene becomes about 19 and 42 times faster, respectively. Tetrahydrofuran contains activated α-C−H bonds and reacts with $[Ru^{VI}(Por)(NTs)_2]$ more rapidly than ethylbenzenes (cf. entries 19 vs 53, 24 vs 57, and 26 vs 58 in Table 4). The k_2 for the amidation of tetrahydrofuran is about 23-fold larger for $[Ru^{VI}(TPP)(NTs)_2]$ than for $[Ru^{VI}(TMP)(NTs)_2]$, in contrast to the about 11-fold larger k_2 value for amidation of ethylbenzene by $[Ru^{VI}(TPP)(NTs)_2]$ than by $[Ru^{VI}(TMP)(NTs)_2]$, indicating a stronger dependence of imido transfer rates on the porphyrin substituents in the case of tetrahydrofuran.

$[Ru^{VI}(TMP)(NCs)_2]$ and $[Ru^{VI}(TPP)(NTs)_2]$ have essentially the same $E_{1/2}(Ru^{VI/V})$ value (−0.27 V vs $Cp_2Fe^{+/0}$, Table 1). Thus, in the absence of steric effect, the reactions of these two imido complexes with a given hydrocarbon should exhibit similar k_2 values. We found that the steric effect in styrene aziridination by $[Ru^{VI}(Por)(NSO_2R)_2]$ is small, with the k_2 for $[Ru^{VI}(TMP)(NCs)_2]$ ($(11.5 \pm 0.6) \times 10^3$, entry 4 in Table 4) comparable to that for $[Ru^{VI}(TPP)(NTs)_2]$ ($(9.0 \pm 0.1) \times 10^3$).[30b] Including $[Ru^{VI}(TPP)(NTs)_2]$, $[Ru^{VI}(2,6\text{-}Cl_2TPP)(NTs)_2]$, $[Ru^{VI}(F_{20}\text{-}TPP)(NTs)_2]$, as well as $[Ru^{VI}(TMP)(NSO_2R)_2]$ (SO_2R = Ms, Ts, Bs, Cs, Ns) in the log k_2 versus $E_{1/2}(Ru^{VI/V})$ plot for styrene aziridination gives a fairly good linearity (Figure S12); the obtained slope (5.5 V^{-1}) is similar to that (5.9 V^{-1}) for $[Ru^{VI}(TMP)(NSO_2R)_2]$ (SO_2R = Ms, Ts, Bs, Cs, Ns) (Figure 6a).

Upon replacing $[Ru^{VI}(TMP)(NCs)_2]$ with $[Ru^{VI}(TPP)(NTs)_2]$, the k_2 becomes about 3-, 6-, 9-, and 20-fold larger for amidation of toluene, ethylbenzene, tetrahydrofuran, and cumene, respec-

tively (cf. entries 47 vs 51, 21 vs 26, 55 vs 58, and 31 vs 34 in Table 4). This can be rationalized by the increasing steric effect along the series toluene (1° C−H) → ethylbenzene, tetrahydrofuran (2° C−H) → cumene (3° C−H). The substantial 20-fold increase in k_2 value for cumene reveals that steric effect could significantly affect the amidation of the 3° C−H bond.

On the basis of the studies described above, it can be envisaged that [Ru^{VI}(F_{20}-TPP)($NNs)_2$] bearing electron-deficient, sterically unencumbered F_{20}-TPP ligand and having strongly electron-withdrawing NO_2 substituent on the imido group should exhibit a high reactivity toward hydrocarbons. Such a complex has not been obtained in pure form but could be generated in situ from reaction of [Ru^{II}(F_{20}-TPP)(CO)] with PhI═NNs in CH_2Cl_2 as mentioned above. Indeed, the reaction of the in situ generated [Ru^{VI}(F_{20}-TPP)($NNs)_2$] with any of the hydrocarbons in Tables 3 and 4 is too fast to be monitored by UV−vis spectrophotometry. Preliminary examination of the [Ru^{II}(F_{20}-TPP)(CO)]-catalyzed amidation of cyclohexane and decalin with PhI═NNs in CH_2Cl_2 at 40 °C with a catalyst:(PhI═NNs):substrate molar ratio of 1:50:5000 afforded the amidation products in 14 and 24% yield (based on the amount of consumed PhI═NNs), respectively (for decalin, a mixture of two isomers in 2.2:1 ratio was obtained); no amidation products could be detected if PhI═NNs was replaced with PhI═NTs.

Conclusion

(i) [Ru^{VI}(Por)($NSO_2R)_2$] is isolable for a series of SO_2R groups and porphyrin ligands. This unique class of metal imido complexes readily undergo imido transfer reactions with hydrocarbons, affording aziridines or amides in good yields. (ii) The reactivity of [Ru^{VI}(Por)($NSO_2R)_2$] toward hydrocarbons is remarkably affected by the electronic properties of the remote *para*-substituents of SO_2R groups; the imido substituent having a larger electron-withdrawing strength results in a higher reactivity. (iii) In terms of the effect of imido substituents, the attack of the imido groups toward alkene double bonds is electrophilic, which complements previous results obtained from the effect of alkene substituents.[30b] (iv) For the amidation of hydrocarbons by [Ru^{VI}(Por)($NSO_2R)_2$], the second-order rate constants correlate with C−H bond dissociation energies, providing additional evidence for the H-atom abstraction mechanism proposed in previous work.[30b] (v) [Ru^{VI}(Por)-($NSO_2R)_2$] shows $Ru^{VI/V}$ reduction at a potential considerably more anodic than [Ru^{VI}(Por)O_2]; more strongly electron-withdrawing imido groups lead to more anodic reduction potentials. The $Ru^{VI/V}$ reduction of [Ru^{VI}(Por)($NSO_2R)_2$] is reversible, whereas that of [Ru^{VI}(TMP)O_2] is irreversible. There is a linear correlation between log k_2 and the $E_{1/2}$($Ru^{VI/V}$) of [Ru^{VI}(Por)($NSO_2R)_2$] for their reaction with styrene, cumene, ethylbenzene, tetrahydrofuran, or toluene (a more anodic $E_{1/2}$($Ru^{VI/V}$) corresponds to a higher reactivity). (vi) Amidation of hydrocarbons by [Ru^{VI}(Por)($NSO_2R)_2$] features larger steric effect than the aziridination of styrene by the same imido complex. Manipulation of the steric hindrance of the imido complexes can reverse the relative amidation reactivity of 3° versus 2°/1° C−H bonds.

Experimental Section

Preparation of [Ru^{VI}(Por)($NSO_2R)_2$]. These complexes were prepared by a modification of the procedure reported previously for the preparation of [Ru^{VI}(Por)($NTs)_2$].[30b] A mixture of [Ru^{II}(Por)(CO)] (0.05 mmol) and PhI═NSO_2R (0.2 mmol) in freshly distilled CH_2Cl_2 (8 mL) was stirred for 5 min at room temperature under argon. The reaction mixture was passed through a short column of neutral alumina with CH_2Cl_2 as eluent. The first band was collected, and the solvent was removed in vacuo, affording the desired product as a dark purple solid in about 70% yield.

[Ru^{VI}(TMP)($NMs)_2$]. Anal. Calcd for $C_{70}H_{66}N_6O_6RuS_2$: C, 67.13; H, 5.31; N, 6.71. Found: C, 67.01; H, 5.12; N, 6.58. UV−vis (3.86×10^{-6} M, CH_2Cl_2): λ_{max}/nm (log ϵ) 422 (5.24), 536 (4.31), 566 (3.55). IR (KBr, cm^{-1}): 1017 ("oxidation state marker" band). ^{1}H NMR (300 MHz, CD_2Cl_2): δ H_β 8.70 (8H, s), H_m(eq) 7.33 (8H, s), *p*-Me(eq) 2.66 (12H, s), *o*-Me(eq) 1.84 (24H, s), H_m(ax) 5.87 (4H, d, J = 8.9 Hz), H_o(ax) 4.91 (4H, d, J = 8.9 Hz), OMe(ax) 3.47 (6H, s). ESMS (CH_2Cl_2): m/z 1252 $[M]^+$, 896 $[M - NMs - Ms]^+$.

[Ru^{VI}(TMP)($NTs)_2$]. Anal. Calcd for $C_{70}H_{66}N_6O_4RuS_2$: C, 68.88; H, 5.45; N, 6.89. Found: C, 68.92; H, 5.38; N, 6.60. UV−vis (5.29×10^{-6} M, CH_2Cl_2): λ_{max}/nm (log ϵ) 421 (5.24), 536 (4.33), 566 (3.63). IR (KBr, cm^{-1}): 1017 ("oxidation state marker" band). ^{1}H NMR (300 MHz, CD_2Cl_2): δ H_β 8.67 (8H, s), H_m(eq) 7.30 (8H, s), *p*-Me(eq) 2.62 (12H, s), *o*-Me(eq) 1.80 (24H, s), H_m(ax) 6.17 (4H, d, J = 8.3 Hz), H_o(ax) 4.81 (4H, d, J = 8.3 Hz), Me(ax) 1.88 (6H, s). ESMS (CH_2Cl_2): m/z 1220 $[M]^+$, 896 $[M - NTs - Ts]^+$.

[Ru^{VI}(TMP)($NBs)_2$]. Anal. Calcd for $C_{68}H_{62}N_6O_4RuS_2$: C, 68.49; H, 5.24; N, 7.05. Found: C, 68.32; H, 5.08; N, 6.97. UV−vis (1.14×10^{-5} M, CH_2Cl_2): λ_{max}/nm (log ϵ) 420 (5.24), 536 (4.28), 566 (3.87). IR (KBr, cm^{-1}): 1017 ("oxidation state marker" band). ^{1}H NMR (300 MHz, CD_2Cl_2): δ H_β 8.69 (8H, s), H_m(eq) 7.31 (8H, s), *p*-Me(eq) 2.63 (12H, s), *o*-Me(eq) 1.81 (24H, s), H_p(ax) 6.80 (2H, t, J = 7.5 Hz), H_m(ax) 6.39 (4H, t, J = 7.9 Hz), H_o(ax) 4.93 (4H, d, J = 7.4 Hz). ESMS (CH_2Cl_2): m/z 1192 $[M]^+$, 896 $[M - NBs - Bs]^+$.

[Ru^{VI}(TMP)($NCs)_2$]. Anal. Calcd for $C_{68}H_{60}Cl_2N_6O_4RuS_2$: C, 64.75; H, 4.79; N, 6.66. Found: C, 64.53; H, 4.71; N, 6.58. UV−vis (5.25×10^{-6} M, CH_2Cl_2): λ_{max}/nm (log ϵ) 419 (5.24), 535 (4.27), 565 (3.54). IR (KBr, cm^{-1}): 1016 ("oxidation state marker" band). ^{1}H NMR (300 MHz, CD_2Cl_2): δ H_β 8.69 (8H, s), H_m(eq) 7.31 (8H, s), *p*-Me(eq) 2.62 (12H, s), *o*-Me(eq) 1.80 (24H, s), H_m(ax) 6.38 (4H, d, J = 8.7 Hz), H_o(ax) 4.87 (4H, d, J = 8.7 Hz). ESMS (CH_2Cl_2): m/z 1262 $[M]^+$, 896 $[M - NCs - Cs]^+$.

[Ru^{VI}(TMP)($NNs)_2$]. Anal. Calcd for $C_{68}H_{60}N_8O_8RuS_2$: C, 63.68; H, 4.72; N, 8.74. Found: C, 63.33; H, 4.61; N, 8.54. UV−vis (2.89×10^{-6} M, CH_2Cl_2): λ_{max}/nm (log ϵ) 416 (5.24), 535 (4.21), 565 (3.68). IR (KBr, cm^{-1}): 1017 ("oxidation state marker" band). ^{1}H NMR (300 MHz, CD_2Cl_2): δ H_β 8.71 (8H, s), H_m(eq) 7.34 (8H, s), *p*-Me(eq) 2.65 (12H, s), *o*-Me(eq) 1.83 (24H, s), H_m(ax) 7.27 (4H, d, J = 8.8 Hz), H_o(ax) 5.18 (4H, d, J = 8.8 Hz). ESMS (CH_2Cl_2): m/z 1282 $[M]^+$, 896 $[M - NNs - Ns]^+$.

[Ru^{VI}(2,6-Cl_2TPP)($NTs)_2$]. Anal. Calcd for $C_{58}H_{34}Cl_8N_6O_4RuS_2$: C, 52.47; H, 2.58; N, 6.33. Found: C, 52.50; H, 2.45; N, 6.18. UV−vis (5.30×10^{-6} M, CH_2Cl_2): λ_{max}/nm (log ϵ) 422 (5.24), 534 (4.26). IR (KBr, cm^{-1}): 1018 ("oxidation state marker" band). ^{1}H NMR (400 MHz, CD_2Cl_2): δ H_β 8.83 (8H, s), $H_{m,p}$(eq) 7.87 (12H, m), H_m(ax) 6.23 (4H, d, J = 8.2 Hz), H_o(ax) 4.86 (4H, d, J = 8.3 Hz), Me(ax) 1.94 (6H, s). ESMS (CH_2Cl_2): m/z 1328 $[M]^+$, 1004 $[M - NTs - Ts]^+$.

[Ru^{VI}(F_{20}-TPP)($NTs)_2$]. Anal. Calcd for $C_{58}H_{22}F_{20}N_6O_4RuS_2$: C, 49.34; H, 1.57; N, 5.95. Found: C, 49.65; H, 1.82; N, 6.21. UV−vis (6.1×10^{-6} M, CH_2Cl_2): λ_{max}/nm (log ϵ) 418 (5.40), 528 (4.38), 558 (3.84). IR (KBr, cm^{-1}): 1019 ("oxidation state marker" band). ^{1}H NMR (300 MHz, CD_2Cl_2): δ H_β 9.01 (8H, s), H_m(ax) 6.28 (4H, d, J = 8.1 Hz), H_o(ax) 4.82 (4H, d, J = 8.2 Hz), Me(ax) 1.99 (6H, s). ^{19}F NMR (376 MHz, CD_2Cl_2): δ *o*-F −135.5 (8F, d, J = 20 Hz), *p*-F −150.7 (4F, t, J = 21 Hz), *m*-F −161.1 (8F, t, J = 22 Hz). ESMS (CH_2Cl_2): m/z 1412 $[M]^+$, 1088 $[M - NTs - Ts]^+$.

[Ru^{VI}(F_{20}-TPP)($NNs)_2$]. This complex was prepared in situ by stirring a solution of [Ru^{II}(F_{20}-TPP)(CO)] (0.05 mmol) and PhI═NNs (0.2 mmol) in CH_2Cl_2 (8 mL) for 5 min at room temperature under

argon. UV−vis (CH_2Cl_2): λ_{max}/nm 413 (Soret), 528. ^{1}H NMR (300 MHz, CD_2Cl_2): δ H_β 9.20 (8H, s), H_m(ax) 7.42 (4H, d, J = 8.7 Hz), H_o(ax) 5.15 (4H, d, J = 8.7 Hz). ESMS (CH_2Cl_2): m/z 1474 $[M]^+$, 1088 $[M - NNs - Ns]^+$.

Stoichiometric Alkene Aziridination and C−H Bond Amidation by [Ru^{VI}(Por)(NSO$_2$R)$_2$]. These reactions were performed under argon using standard Schlenk techniques. A typical procedure is given as follows: To a solution of substrate (1 or 2 mmol) in CH_2Cl_2 (2 mL) in a Schlenk tube (10 mL) were added [Ru^{VI}(Por)(NSO$_2$R)$_2$] (0.05 mmol) and pyrazole (2% w/w). The mixture was stirred for 3 h. After removal of solvent in vacuo, a mixture of *n*-pentane and Et_2O (5:1 v/v, 20 mL) was added, resulting in the formation of a reddish−purple precipitate. The precipitate was found to be [Ru^{IV}(Por)(NHSO$_2$R)(pz)] (yield: about 65%), which was collected by filtration and washed with *n*-pentane. The filtrate containing organic products was evaporated to dryness, and the residue was dissolved in ethyl acetate and purified by chromatography. The organic products were identified as described in Supporting Information.

[Ru^{IV}(TMP)(NHMs)(pz)]. Anal. Calcd for $C_{66}H_{63}N_7O_3RuS$: C, 69.82; H, 5.59; N, 8.64. Found: C, 69.62; H, 5.85; N, 8.90. UV−vis (4.05×10^{-6} M, CH_2Cl_2): λ_{max}/nm (log ϵ) 414 (5.26), 529 (4.20), 560 (3.95, sh). IR (KBr, cm^{-1}): 1010 ("oxidation state marker" band). ^{1}H NMR (300 MHz, CD_2Cl_2): δ H_β −17.5 (8H, s), H_m(eq) 6.17 (8H, d), *p*-Me(eq) 2.04 (12H, s), *o*-Me(eq) 1.55 (24H, s), H_m(ax) 10.9 (2H, s), H_o(ax) 5.0 (2H, s), *p*-OMe(ax) 4.65 (3H, s), pz −25.0 (1H, s) and −27.7 (1H, s) (the signal of the ortho proton was not located). FAB MS: m/z 1136 $[M + H]^+$, 1068 $[M - pz]^+$, 882 $[M - NHMs - pz]^+$.

[Ru^{IV}(TMP)(NHCs)(pz)]. Anal. Calcd for $C_{65}H_{60}ClN_7O_2RuS$: C, 68.49; H, 5.31; N, 8.60. Found: C, 68.43; H, 5.30; N, 8.43. UV−vis (4.39×10^{-6} M, CH_2Cl_2): λ_{max}/nm (log ϵ) 413 (5.29), 528 (4.23), 561 (3.99, sh). IR (KBr, cm^{-1}): 1009 ("oxidation state marker" band). ^{1}H NMR (400 MHz, CD_2Cl_2): δ H_β −18.6 (8H, s), H_m(eq) 6.16 (8H, d), *p*-Me(eq) 2.04 (12H, s), *o*-Me(eq) 1.57 (24H, s), H_m(ax) 11.9 (2H, s), H_o(ax) 5.1 (2H, s), pz −25.8 (1H, s) and −27.8 (1H, s) (the signal of the ortho proton was not located). ESMS (CH_2Cl_2): m/z 1139 $[M]^+$, 1072 $[M - pz]^+$, 882 $[M - NHCs - pz]^+$.

[Ru^{IV}(TMP)(NHNs)(pz)]. Anal. Calcd for $C_{65}H_{60}N_8O_4RuS$: C, 67.87; H, 5.26; N, 9.74. Found: C, 68.05; H, 5.09; N, 9.54. UV−vis (5.73×10^{-6} M, CH_2Cl_2): λ_{max}/nm (log ϵ) 411 (5.05), 531 (3.93), 560 (3.69). IR (KBr, cm^{-1}): 1010 ("oxidation state marker" band). ^{1}H NMR (300 MHz, CD_2Cl_2): δ H_β −19.7 (8H, s), H_m(eq) 6.11 (8H, d), *p*-Me(eq) 2.00 (12H, s), *o*-Me(eq) 1.56 (24H, s), H_m(ax) 12.7 (2H, s), H_o(ax) 5.1 (2H, s), pz −26.8 (1H, s) and −28.8 (1H, s) (the signal of the ortho proton was not located). ESMS (CH_2Cl_2): m/z 1150 $[M]^+$, 1083 $[M - pz]^+$, 882 $[M - NHNs - pz]^+$.

[Ru^{IV}(F$_{20}$-TPP)(NHTs)(pz)]. Anal. Calcd for $C_{54}H_{19}F_{20}N_7O_2RuS$: C, 49.48; H, 1.46; N, 7.48. Found: C, 49.20; H, 1.76; N, 7.75. UV−vis (6.21×10^{-6} M, CH_2Cl_2): λ_{max}/nm (log ϵ) 407 (5.18), 525 (4.15). IR (KBr, cm^{-1}): 1015 ("oxidation state marker" band). ^{1}H NMR (300 MHz, $CDCl_3$): δ H_β −15.0 (8H, s), H_m(ax) 12.3 (2H, s), H_o(ax) 4.8 (2H, s), Me(ax) 11.8 (3H, s) (the pz signals were not located). FAB MS: m/z 1312 $[M + H]^+$, 1244 $[M - pz]^+$, 1074 $[M - NHTs - pz]^+$.

X-ray Crystal Structure Determination of [Ru^{IV}(TMP)(NHCs)(pz)]·5H$_2$O. A diffraction-quality crystal ($0.25 \times 0.2 \times 0.06$ mm^3), obtained by slow evaporation of a $CHCl_3$−MeOH solution (1:3 v/v) at room temperature for 3 days, was mounted on a glass fiber for data collection at 28 °C on a MAR diffractometer with a 300 mm image plate detector using graphite-monochromatized Mo Kα radiation (λ = 0.71069 Å) (2° oscillation, 66 images at 120 mm distance and 600 s exposures). The images were interpreted and intensities integrated by using DENZO.[46] The structure was solved by direct methods employing SIR-97[47] on PC and expanded by Fourier cycles and refined by full-matrix least-squares using SHELXL-97.[48] A crystallographic asymmetric unit consists of one formula unit. In the least-squares refinement, Ru, S, Cl, O, and N atoms in the molecule were refined anisotropically and other non-hydrogen atoms isotropically. The positions of H-atoms were calculated based on riding mode with thermal parameters equal to 1.2 times that of the associated C atoms and participated in the calculation of the final R indices.

Kinetic Studies. These were performed by following the procedures reported previously.[30b]

Acknowledgment. This work was supported by The University of Hong Kong, the Hong Kong Research Grants Council (HKU7011/04P), University Development Fund of the Hong Kong University, and the University Grants Committee of the Hong Kong SAR of China (Area of Excellent Scheme, AoE/P-10/01).

Supporting Information Available: General Experimental Section, characterization of aziridination/amidation products, Figures S1−S12, and CIF file for the X-ray crystal structure of [Ru^{VI}(TMP)(NHCs)(pz)]·5H$_2$O. This material is available free of charge via the Internet at http://pubs.acs.org.

JA0542789

(46) Otwinowski, Z.; Minor, W. In *Methods in Enzymology, Vol. 276: Macromolecular Crystallography, Part A*; Carter, C. W., Jr., Sweet, R. M., Eds.; Academic Press: New York, 1997; p 307.
(47) Altomare, A.; Burla, M. C.; Camalli, M.; Cascarano, G.; Giacovazzo, C.; Guagliardi, A.; Moliterni, A. G. G.; Polidori, G.; Spagna, R. *J. Appl. Crystallogr.* **1999**, *32*, 115.
(48) Sheldrick, G. M. *SHELXL-97. Program for the Refinement of Crystal Structures*. University of Götingen: Göttingen, Germany, 1997.